Large inelastic deformation resistance of stiffened panels subjected to lateral loading

Zhaolong Yu [a, b], Jørgen Amdahl [a, b], Yanyan Sha [a, b*]

a. Department of Marine Technology, Norwegian University of Science and Technology (NTNU)

b. Centre for Autonomous Marine Operations and Systems (AMOS), NTNU

Abstract

This paper presents a simplified formulation for the assessment of large deformation resistance of stiffened panels subjected to lateral loading. The method is based on rigid plastic material assumptions and the use of yield functions formulated in terms of stress resultants. The method considers the flexibility of the panel ends with respect to inward motion, while the rotational boundary conditions are free or clamped. Concentrated and distributed loads are considered, as is patch loading. The resistance-deformation curves predicted by the proposed method are compared with results from experiments and using LS-DYNA, and good agreement is obtained for panels that are not dominated by shear failure and tripping or local buckling of stiffeners at the early stage of deformation. The formulation provides a useful tool for quick estimates of panels subjected to abnormal or accidental static and transient lateral loads such as ship collisions, dropped objects, explosions, slamming, hydrostatic pressure and ice actions.

Key words: stiffened panels; abnormal lateral loads; large deformation resistance; plastic analysis; axial inward motion

1. Introduction

Stiffened panels are widely used in ships, offshore platforms and other engineering structures. A typical stiffened panel structure on a ship side or bottom is shown in Fig. 1. Such structures are often exposed to the risk of explosions, ship collisions, violent water slamming, ice pressure and impacts from dropped objects. Potential consequences may vary from minor local deformation to major structural damage and plate rupture, causing compartment flooding or oil leakage. In extreme cases, the loads may cause the entire structure to collapse and put human lives in jeopardy. Consequently, it is crucial to estimate the resistance and damage of stiffened panels with good efficiency and accuracy, notably when they are loaded to their extreme performance limits during accidental events.

Several methods are available for structural response analysis, including nonlinear finite element methods (NLFEM) [1, 2], experimental methods and simplified methods. In the design stage, a number of scenarios and structural configurations need to be assessed. For this purpose, nonlinear finite element analysis is not practical due to significant modeling efforts and computational costs. Experimental methods will provide accurate results if the scaling law is properly handled, but the disadvantages include high cost and a long period of time from test preparation to results. Thus, simple analytical methods that can perform a quick and realistic assessment of the resistance during inelastic deformations are desired. A few design standards contain simple resistance expressions, such as DNV RP C204 [3] and the NORSOK N004 standard [4].

* Corresponding author, Yanyan Sha, email: yanyan.sha@ntnu.no

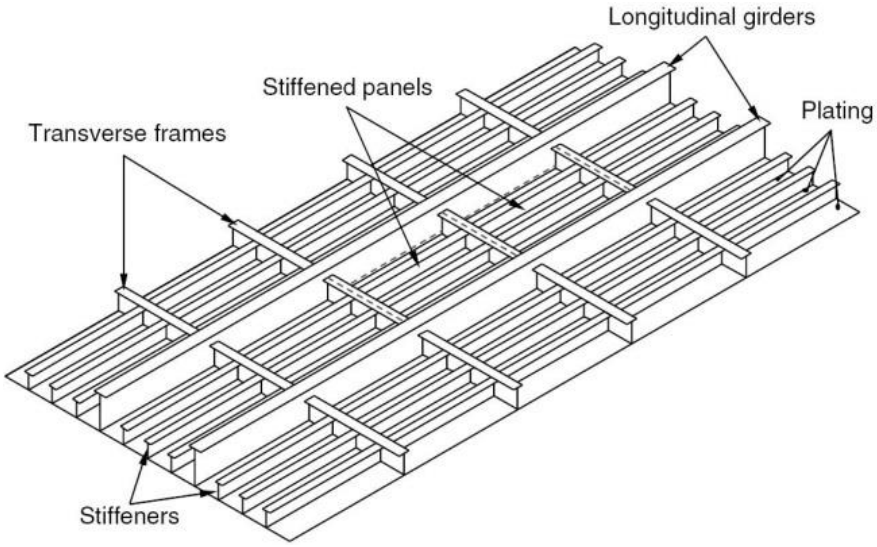

Fig. 1. Stiffened panel

Numerous formulations of the resistance and energy dissipation of structural components and subassemblies during accidental actions are available in the literature. They are typically based on plastic theory and the assumption of idealized deformation modes inspired by deformation patterns observed in actual accidents, model tests or numerical simulations. Wierzbicki and Abramowicz [5] presented pioneering work on the crushing resistance of thin-walled structures. Amdahl [6] derived simplified formulas for the crushing resistance of a ship bow. Jones [7] presented useful analytical models for the impact response of beams, plates and shells. Both static and dynamic responses were addressed. The effects of transverse shear and rotatory inertia were discussed.

As for the deformation resistance of stiffened panels, a simple way to address stiffened panels may be to smear the thickness of stiffeners onto the attached plate, but the accuracy was shown to be crude [8]. Considering the confinement effect in the longitudinal and transverse directions, the deformation resistance models of stiffened panels under blast loads can be found in refs. [9-12]. For beam deformation of stiffened panels with only longitudinal confinement, Schubak et al. [13, 14] and Yang and Peng [15] presented rigid plastic models with clamped ends and partial end fixity subjected to uniformly distributed blast loads. However, the neutral axis was assumed to coincide with the centroid axis. The resulting yield curve was asymmetric and was simplified as a linear piecewise curve, which is not accurate. The DNV RP C204 [3] standard presented the static resistance of laterally deflected stiffened frames by using a practical approximation of the interaction function of the bending moment and the membrane force. Amdahl [16] proposed a model for the resistance of stiffened panels with fixed end conditions subjected to explosions with more refined yield functions. Daley et al. [17] presented a model for overload response of simple flat bar stiffened frames subjected to ice loading, and the effect of bending and shear is discussed while the axial force is neglected. A series of full-scale experiments for the lateral indentation resistance of single stiffened frames and ship grillages were conducted and reported

by Daley and Hermanski [18] and Kim [19], which provide valuable results for the investigation of the ultimate strength of stiffened frames.

Considering the flexibility of beam ends, Jones [20] proposed an analytical formulation that accounted for the effect of inward flexibility of beam ends. A drawback to this method was that the flexibility was proportional to the square of the deflection, which made it difficult to associate it with the physical properties of a structure. Hodge [21] and De Oliveria [22] presented simple expressions for the resistance of rectangular and tubular beams respectively under lateral loading, and boundary translational and rotational flexibilities were accounted for. They showed that the translational stiffness of beam ends was crucial for the development of membrane forces in large deformation conditions

This paper presents a simplified formulation for the large beam-deformation resistance of stiffened panels with T-profile and L-profile stiffeners. The effects of distributed loads, different loading positions and boundary translational and rotational stiffness are accounted for. Results from experiments and numerical simulations are used to verify the proposed analytical model. A number of cases are simulated with LS-DYNA, covering a broad range of impact scenarios. The shear and dynamic inertia effects are discussed as well. The proposed model may serve as design equations in the design standards of marine structures.

2. Yield functions based on generalized forces

The object of this study is a stiffened panel with a vertically asymmetric I-profile, as shown in Figs. 1 and 2 (a). The areas of the plate flange, the top flange and the stiffener web are denoted A_p, A_t and A_w, respectively. h_w denotes the height of the web. It is presupposed that the area of the plate flange is larger than or equal to the area of the small flange and the web such that $A_p \geq A_w + A_t$. This assumption is valid for most stiffened panels used in ships and offshore installations. The material is assumed to be rigid perfectly plastic with a yield strength of σ_y .

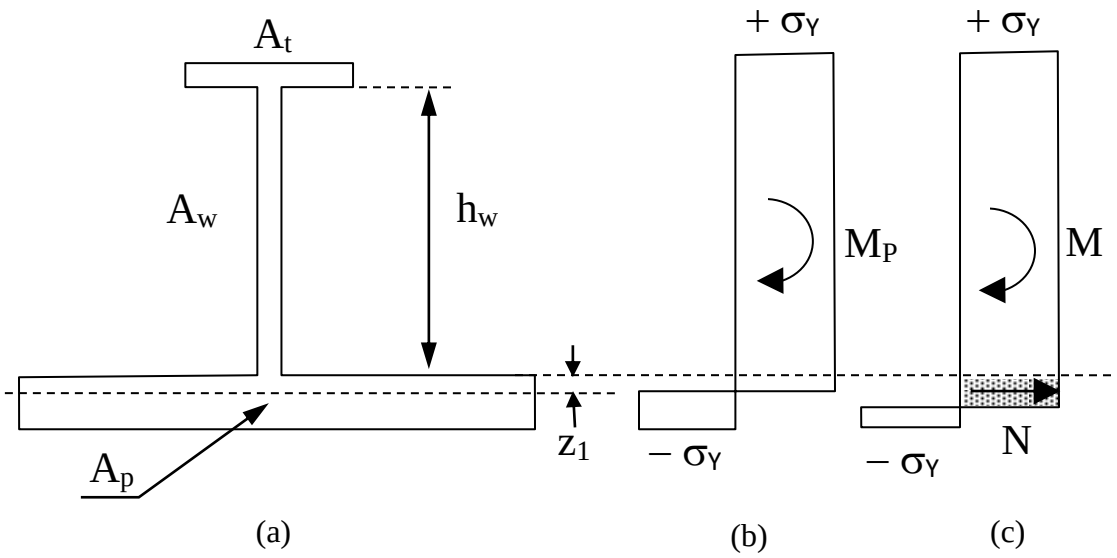

Fig. 2. Stiffened panel cross section subjected to bending and tension

First, pure bending of the cross section is considered. The stress distribution in the fully plastic state is shown in Figure 2(b). The plastic neutral axis is located such that it divides the cross section into two equal areas. This implies that the axis is initially located in the plate flange, given by the coordinate z_1 :

$$\frac{z_1}{t_p} = \frac{A_p - A_w - A_t}{2A_p} = 1 - \frac{A_e}{2A_p} \tag{1}$$

where t_p is the thickness of the plate flange and A_e is the total area of the stiffened panel cross section, i.e. $A_e = A_p + A_w + A_t$. As the area relation of $A_p \geq A_w + A_t$ is assumed, z_1 must always be smaller than $\frac{t_p}{2}$; i.e. $2z_1 < t_p$.

The following approximations are introduced in the calculation of the plastic bending moment:

- The contribution from the large bottom plate is small because the plastic neutral axis is located in the plate flange.
- The distance to the neutral axis, z_1 , in the plate flange is neglected.
- The thickness of the stiffener top flange is assumed to be small compared to the web height, h_w and is neglected.

The fully plastic bending moment is approximately:

$$M_p = \sigma_y \left(A_w \frac{h_w}{2} + A_t h_w \right) \tag{2}$$

In deriving the interaction functions, the effect of shear deformation is assumed to be negligible. If the cross section that is fully plasticized in bending is subjected to an increasing membrane tension force, as shown in Figure 2(c), a part of the compression field below the plastic neutral axis, z_1 , has to change to yielding in tension. An equal area of the tension field above the plastic neutral axis will be "occupied" by the axial force, N . The total area "occupied" by the tension force is indicated by the shaded area in Figure 2(c). Depending on the magnitude of the axial force, the stiffened panel response may be classified into four different stages.

Stage 1: Tension force in the plate flange only

As long as the tension force occupies the plate flange only, the bending moment is not affected. The limiting axial force N^* is given by:

$$\frac{N^*}{N_P} = \frac{A_p - A_w - A_t}{A_e} = 2\frac{A_p}{A_e} - 1 \tag{3}$$

where N_p is the plastic collapse force of the cross section in tension; $N_p = \sigma_y A_e$.

Hence, the following interaction applies:

$$F = \frac{M}{M_P} - 1 = 0, \qquad \frac{N}{N_P} \le \frac{N^*}{N_p} \tag{4}$$

An approximation of this interaction could be used:

$$F = \frac{M}{M_P} + \left(\frac{N}{N_p}\right)^n - 1 = 0, \qquad 0 \le \frac{N}{N_P} < \frac{N^*}{N_p} \tag{5}$$

where n takes a large value.

Stage 2: Tension force in the plate flange and web

In this stage, the axial force reaches such a level that it also occupies a part of the web in addition to a part of the plate flange, i.e., $N > N^*$. The height of the zone "occupied" by the axial force is denoted z_2 , as shown in Fig. 3.

The plastic interaction relationship becomes:

$$F = \frac{M}{M_p} + \frac{1}{1 + 2\dfrac{A_f}{A_w}}\left(\frac{A_e}{2A_w}\right)^2\left(\frac{N - N^*}{N_p}\right)^2 - 1 = 0 \tag{6}$$

The yield function in Eq. (6) is valid as long as $z_2 < h_w$, which gives:

$$\frac{N^*}{N_P} \le \frac{N}{N_p} \le \frac{N^{**}}{N_P} \tag{7}$$

where N^{**} represents the axial force when the tension force 'occupies' the entire stiffener web, as shown in Fig. 3(c). This gives:

$$\frac{N^{**}}{N_P} = 1 - 2\frac{A_f}{A_e} \tag{8}$$

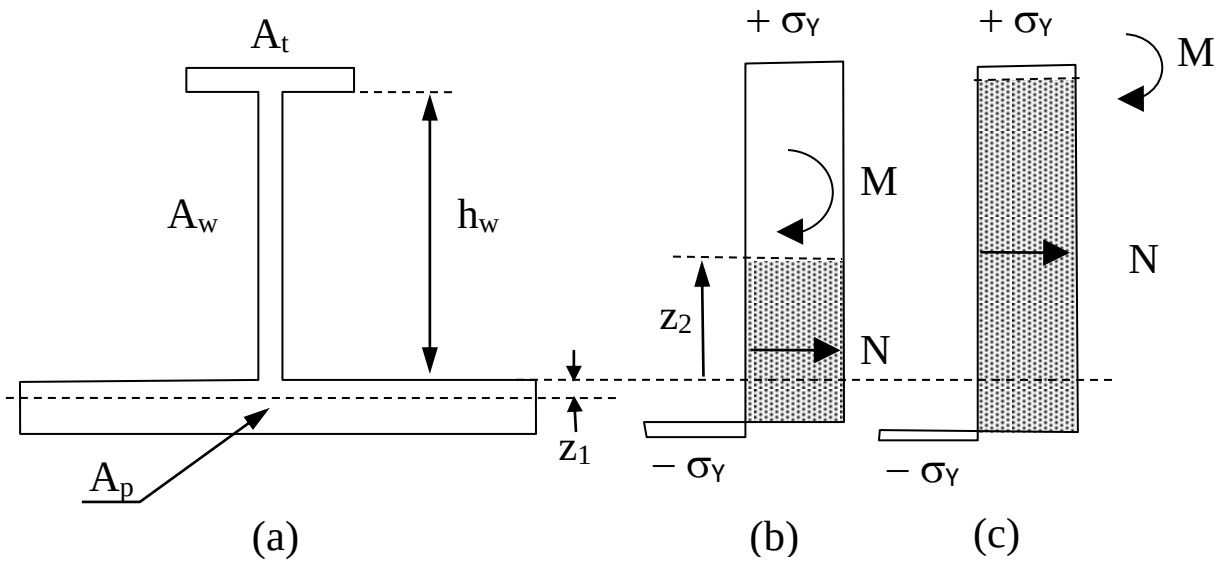

Fig. 3. Plastic stress distribution in stage 2

Stage 3: Tension force in the plate flange, web and top flange

In this stage, the plastic interaction function becomes:

$$F = \frac{M}{M^{**}} + \frac{N - N^{**}}{N_P - N^{**}} - 1 = 0 \tag{9}$$

where $M^{**} = \sigma_y A_t h_w$ is the maximum plastic bending moment from the top flange. The interaction is linear and holds true as long as:

$$\frac{N^{**}}{N_P} < \frac{N}{N_p} \leq 1 \tag{10}$$

Stage 4: Pure tension force

In this stage, the tension force 'occupies' the entire cross section and the bending moment vanishes. The axial force is constant and is:

$$N = N_p \tag{11}$$

Fig. 4 shows the non-dimensional interaction functions of bending moments and axial forces for given A_p / A_s and A_w / A_t ratios. A_s is the sum area of the web and the top flange cross section, i.e. $A_s = A_w + A_t$. The A_p / A_s ratio plays a dominant role in determining the shape of the interaction curves, while the effect of the A_w / A_t ratio is smaller. The interaction curve asymptotically approaches that of a rectangular cross section when $A_p / A_s = 1$ and $A_w / A_t \to \infty$. The interaction becomes more linear for symmetric I-profiles. The present DNV RP C204 [3] expresses the static resistance of laterally deflected stiffened panels by assuming a practical

approximation of the interaction function of bending moment and membrane forces as $M/M_p+\left(N/N_p\right)^{1.2}=1$. The approximation will introduce errors especially when A_p/A_s is large. The interaction function will be updated in the new version DNVGL-RP-C204 standard (version 2018, to be released), and the proposed method in this paper is expected to be included.

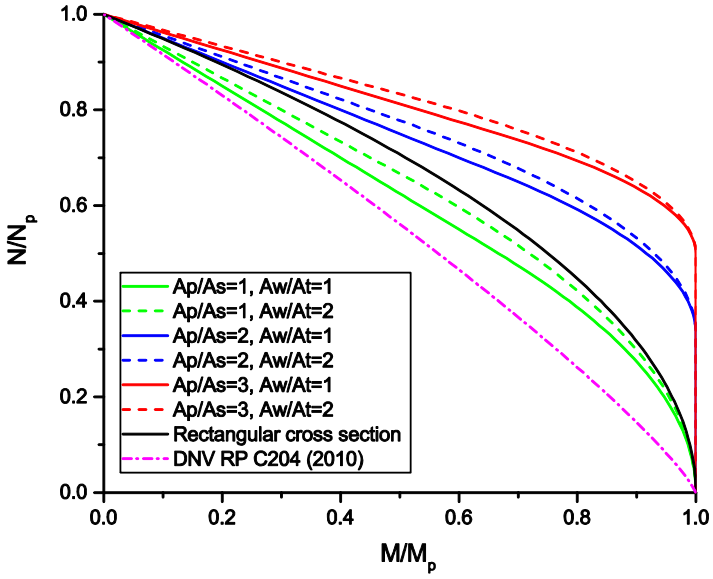

Fig. 4. Non-dimensional interaction functions of bending moment and axial forces

3. Resistance of stiffened panels at finite deformation

3.1 Resistance with fixed boundaries

The large deformation resistance of stiffened panels with T-profile stiffeners in fixed conditions was studied by Amdahl [16]. The formulation is described briefly. The procedure will later be extended to more general scenarios considering different loading positions, distributed loads and translational flexibilities at the boundaries.

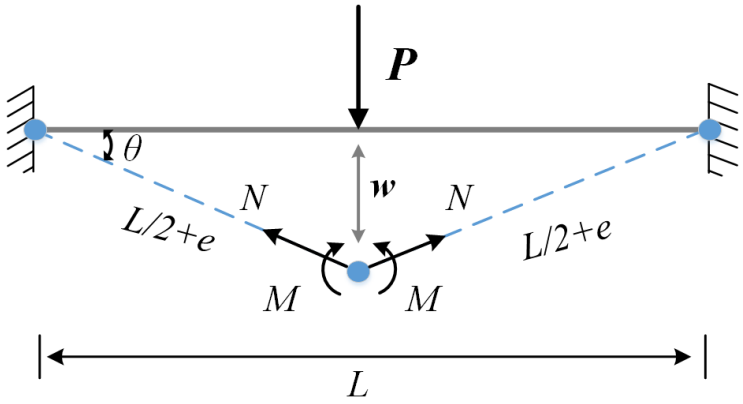

Fig. 5. Beam collapse mechanism for cases with clamped ends

When the lateral load increases, the beam will first collapse via a three-hinge bending mechanism. Subsequently, the membrane force starts to develop and interacts with the bending moment. When the tension force ultimately occupies the entire cross section, the beam behaves like a catenary.

By applying the virtual work principle, the total lateral resistance, P, contains one contribution from bending and the other from the axial force:

$$P = \frac{8M}{L} + 4N\frac{w}{L} \tag{12}$$

where w is the crushing displacement.

The lateral displacement is assumed to be small compared to the total length of the beam. The angle of rotation, θ, and the elongation e, of one half of the beam become:

$$\theta = \frac{2w}{L}; \quad e = \frac{w^2}{L} \tag{13}$$

It is further assumed that the elongation e is distributed equally among the plastic hinges; thus, the virtual elongation and rotation are related by:

$$\begin{aligned} &\delta\theta = \frac{2\delta w}{L}; \quad \delta\left(\frac{e}{2}\right) = \frac{w\delta w}{L} \\ &\delta\left(\frac{e}{2}\right) = \frac{w}{2}\delta\theta \end{aligned} \tag{14}$$

Drucker's postulate (the normality criterion) for plastic flow states that the instantaneous virtual elongation and rotation of the plastic hinges should satisfy:

$$\delta\left(\frac{e}{2}\right) = \delta\lambda\frac{\partial F}{\partial N}; \quad \delta\theta = \delta\lambda\frac{\partial F}{\partial M} \tag{15}$$

This gives:

$$\delta\left(\frac{e}{2}\right) = \frac{\dfrac{\partial F}{\partial N}}{\dfrac{\partial F}{\partial M}}\delta\theta \tag{16}$$

F is the interaction functions.

Utilizing the interaction functions, the kinematic relationship in Eq. (14) and the normality criterion in Eq. (16), a closed-form solution for the resistance versus deformation can be achieved.

For stage 1, it is particularly observed that the interaction function in Eq. (4) does not give a relationship between rotation and elongation using the normality criterion. If Eq. (5) is used, we obtain:

$$w = 2n\frac{M_p}{N_p}\left(\frac{N}{N_p}\right)^{n-1} \to 0; \quad when\ n \to \infty \tag{17}$$

This means that $N^* / N_p \ll 1$. Therefore, we assume $w = 0$ for stage 1, and the resistance is equal to $P_0 = 8M_p / L$, which is identical to the plastic collapse load in pure bending.

In stage 2, the following resistance-deformation relationship is obtained:

$$\frac{P}{P_0} = 1 + \frac{1}{\left(1 + 2\frac{A_t}{A_w}\right)}\left\{\left(\frac{w}{h_w}\right)^2 + \frac{A_p - A_w - A_t}{A_w}\frac{w}{h_w}\right\} \tag{18}$$

It is found that consistency with stage one is automatically satisfied by Eq. (18) when $w = 0$. By satisfying the right side of Eq. (7), we obtain:

$$\frac{w}{h_w} \le 1 \tag{19}$$

In stage 3, the resistance is constant and is equal to:

$$\frac{P}{P_0} = \frac{A_e}{A_w + 2A_t} \tag{20}$$

Eq. (20) in stage 3 applies at only one point, $w = h_w$, and the resistance is consistent with stage 2.

In stage 4, the entire cross section yields in tension. Eq. (12) applies with $M = 0; N = N_p$. The resistance, which is given by:

$$\frac{P}{P_0} = \frac{A_e}{A_w + 2A_t}\frac{w}{h_w} \tag{21}$$

increases linearly with w / h_w .

Normalized resistance-deformation relationships are plotted in Fig. 6 for various ratios of the plate-stiffener area A_p / A_s and the web-top flange area A_w / A_t . It is observed that the resistance increases with increasing ratios of A_p / A_s and A_w / A_t ; the collapse in bending is governed by the plastic section modulus, where the area of the top flange is crucial, but it is the total area that governs the catenary action.

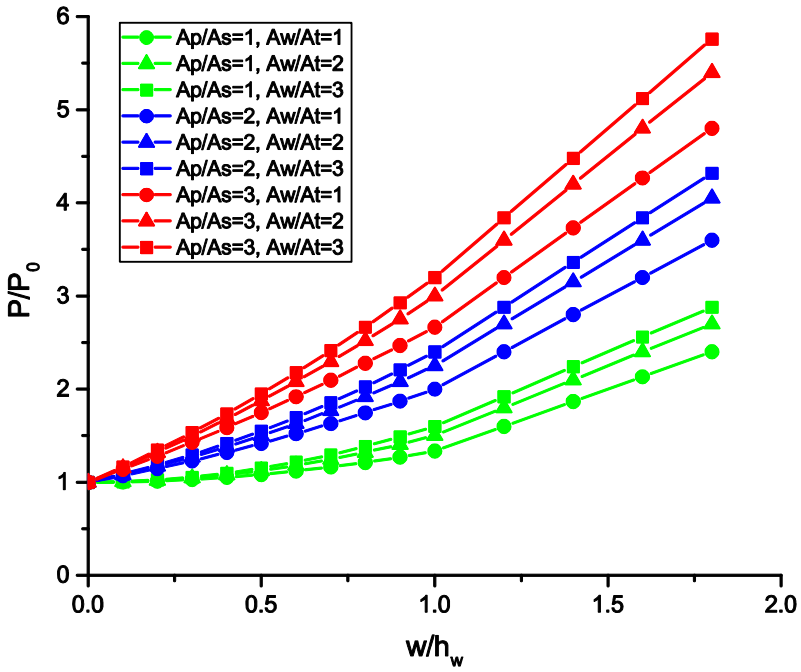

Fig. 6. Non-dimensional resistance versus deformation

3.2 Resistance with finite end restraints

Boundaries with finite end restraints are analyzed. Both clamped and free rotational boundaries are considered. For cases with finite rotational stiffness, it should be distinguished whether or not plastic hinges occur at the supports. In practice, the duration of the elastic rotation stage at the support is short and can be neglected. Consequently, finite rotational restraints will not be considered. A detailed derivation of the effect of rotational restraints on the resistance to lateral deformation of a circular beam can be found in De Oliveria [22].

The stiffened panel is assumed to have a finite stiffness, k , to inward motion at both ends; see Fig. 7. It is loaded with a point load P in the middle. The rotational degree of freedom is assumed to be fixed.

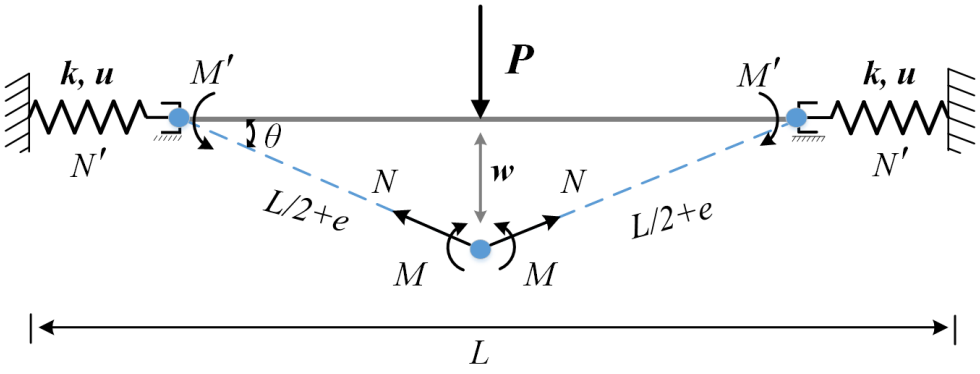

Fig. 7. Beam collapse mechanism with finite translational stiffness

As the deflection, w, is small compared to the beam length, L, the force and moment equilibrium gives:

$$N \approx N'; \quad M \approx M' \tag{22}$$

The following geometrical relationships apply:

$$e = \sqrt{\left(\frac{L}{2} - u\right)^2 + w^2} - \frac{L}{2} \approx \frac{w^2}{L} - u \tag{23}$$

$$\theta \approx \frac{2w}{L} \tag{24}$$

This gives:

$$\delta\left(\frac{e}{2}\right) = \frac{w}{2}\delta\theta - \frac{\delta N}{2k} = \frac{w}{2}\delta\theta - \frac{\delta\left(\frac{N}{N_p}\right)}{\delta\left(\frac{w}{h_w}\right)}\frac{h_w}{2c}\delta\theta \tag{25}$$

where the nondimensional translational spring stiffness factor is defined by:

$$c = \frac{2kh_w^{\,2}}{LN_p} \tag{26}$$

In stage 1, Eq. 4 will not provide a solution to the development of the membrane forces as a function of the displacement. In lieu of that, the interaction equation for stage 2, Eq. 6 is used, but the bending moment remains equal to M_p until the membrane force N reaches N^*. This means that the expression for the membrane force in stage 2 shall pass the point $\left(w = 0,\, N = 0\right)$.

In stage 2, the normality criterion gives:

$$\delta\left(\frac{e}{2}\right) = \frac{1}{1 + 2\frac{A_t}{A_w}}\left(\frac{A_e}{2A_w}\right)^2 \frac{2M_p}{N_p}\left(\frac{N - N^*}{N_p}\right)\delta\theta = \frac{h_w A_e}{4A_w}\left(\frac{N - N^*}{N_p}\right)\delta\theta \tag{27}$$

By combining Eqs. (25) and (27), the governing differential equation for the axial forces in stage 2 reads:

$$\frac{\delta\left(\frac{N}{N_p}\right)}{\delta\left(\frac{w}{h_w}\right)} + \frac{A_e c}{2A_w}\left(\frac{N}{N_p}\right) = c\left(\frac{w}{h_w}\right) + \frac{A_e c}{2A_w}\frac{N^*}{N_p} \tag{28}$$

The axial force N shall vanish for $w = 0$. This gives:

$$\frac{N}{N_p} = \left(\frac{4A_w^{\,2}}{A_e^{\,2} c} - \frac{N^*}{N_p} \right) \exp\left(-\frac{A_e c}{2A_w} \frac{w}{h_w} \right) + \frac{2A_w}{A_e} \frac{w}{h_w} + \frac{N^*}{N_p} - \frac{4A_w^{\,2}}{A_e^{\,2} c} \tag{29}$$

The solution is valid for:

$$0 \le \frac{N}{N_p} \le \frac{N^{**}}{N_P} \tag{30}$$

By substituting Eq. (29) into Eq. (6), the bending moment M is determined for $\frac{N^*}{N_p} \le \frac{N}{N_p} \le \frac{N^{**}}{N_p}$.

For $\frac{N}{N_p} < \frac{N^*}{N_p}$, we have $M = M_p$ according to Eq. (4).

In stage 3, the kinematic relationship, Eq. (25), and the normality criterion give the following differential equation:

$$\frac{\delta\left(\frac{N}{N_p}\right)}{\delta\left(\frac{w}{h_w}\right)} = c\left(\frac{w}{h_w}\right) - c \tag{31}$$

with solution:

$$\frac{N}{N_p} = \frac{1}{2} c \left(\frac{w}{h_w}\right)^2 - c\frac{w}{h_w} + \lambda \tag{32}$$

λ is a constant that is determined from the continuity of Eqs. (29) and (32) at $N = N^{**}$.

N / N_p should be less than or equal to 1 and gives the upper limit of the lateral deflection for stage 3. By substituting Eq. (32) into Eq. (9), the corresponding bending moment M can be found.

In stage 4, the entire cross section fully yields in tension, and the stiffened panel behaves like a catenary. This gives $M = 0; N = N_p$.

It is straightforward to extend the procedure to a beam with rotationally free ends, and the major difference is that the plastic hinges only occur in the mid-section.

If the beam is subjected to a uniform patch load over a distance B, two deformation modes may be considered. If the distributed action is “strong” (e.g., ship collision), the middle hinge will be split into two. The problem may be simplified as a beam with an effective length of $L_{eff} = L - B$ subjected to a concentrated force equal to the resultant of the distributed action.

If the distributed action is “softer”, e.g., hydrodynamic loads and ice loads, the middle hinge may not be split. If the pressure is a uniformly distributed pressure, p, over the entire beam length, the resistance may be estimated with an effective concentrated force $P = 0.5pL$ in accordance with the DNV rules [23] for ice loading. For patch loading, $P = \gamma pL$ may be assumed, with γ varying from 0.5 to 1 depending on the patch loading area.

For cases with different translational stiffnesses at each end, i.e., $k_1 \neq k_2$, an equivalent translational stiffness k_{eq} should be used:

$$\frac{1}{k_{eq}} = \frac{1}{k_1} + \frac{1}{k_2} \tag{33}$$

For a general case with non-central loading as shown in Fig. 8, the non-dimensional translational stiffness factor should be:

$$c = \frac{k_{eq} h_w^{\,2}}{\alpha(1-\alpha) L_{eff} N_p} \tag{34}$$

where:

$$L_1 = \alpha L_{eff};\ L_2 = (1-\alpha) L_{eff} \tag{35}$$

Applying the principle of virtual work, an approximate resistance is obtained:

$$P \approx (\beta M + Nw) \cdot \left(\frac{1}{\alpha L_{eff}} + \frac{1}{1-\alpha\ L_{eff}} \right);\quad \beta = \begin{cases} 1 & \text{free rotation} \\ 2 & \text{fixed rotation} \end{cases} \tag{36}$$

The plastic collapse force in pure bending is:

$$P_0 = \frac{\beta M_p}{\alpha(1-\alpha) L_{eff}} \tag{37}$$

By substituting the obtained axial force N and the bending moment M into Eq. (36), the resistance-displacement curve is readily obtained.

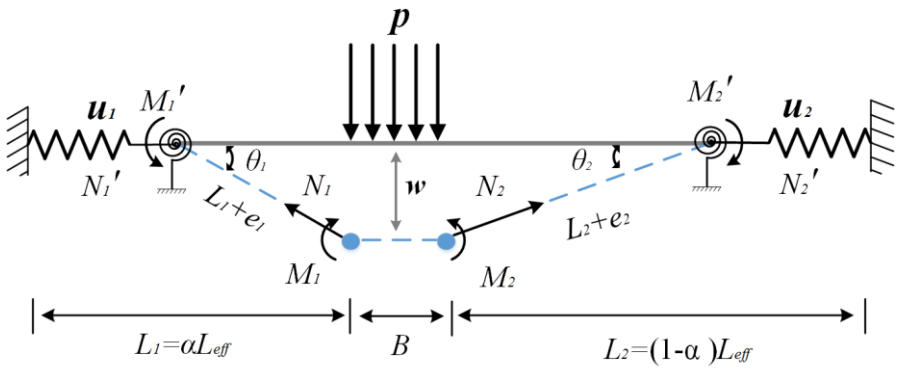

Fig. 8. Beam collapse mechanism in a general loading condition

In summary, the non-dimensional resistance for a general loading case reads:

$$\frac{P}{P_0}=\frac{M}{M_p}+\frac{Nw}{\beta M_p};\quad \beta=\begin{cases}1 & \text{free rotation}\\ 2 & \text{fixed rotation}\end{cases} \tag{38}$$

where:

$$\begin{aligned}
&P_0=\beta M_p\left(\frac{1}{\alpha L_{eff}}+\frac{1}{(1-\alpha)L_{eff}}\right)\\
&M_p=\sigma_y\left(\frac{1}{2}A_w h_w+A_t h_w\right)\\
&N_p=\sigma_y A_e
\end{aligned} \tag{39}$$

The development of the membrane force is determined by:

$$\begin{aligned}
&\frac{N}{N_p}=\left(\frac{16}{\beta^2 c}\left(\frac{A_w}{A_e}\right)^2-\left(2\frac{A_p}{A_e}-1\right)\right)\left[\exp\left(-\frac{\beta c}{4}\frac{A_e}{A_w}\frac{w}{h_w}\right)-1\right]\\
&\qquad+\frac{4}{\beta}\frac{A_w}{A_e}\frac{w}{h_w};\quad \left(stage\,1,2:\frac{N}{N_p}\le 1-\frac{2A_t}{A_e}\right)\\
&\frac{N}{N_p}=\left(\frac{1}{2}c\left(\frac{w}{h_w}\right)^2-\frac{\beta c}{2}\frac{w}{h_w}+\lambda\right);\quad \left(stage\,3:1-\frac{2A_t}{A_e}\le\frac{N}{N_p}<1\right)\\
&\frac{N}{N_p}=1;\quad stage\,4
\end{aligned} \tag{40}$$

c is the non-dimensional stiffness factor; refer to Eq. (34).

λ is a constant that should be determined by the continuity of axial forces at $N=N^{**}$.

From Fig. 4, the slope of the interaction curve in stage 2 does not change much compared to that in stage 3. Therefore, it is reasonable to extend Eq. (29) for the development of axial forces in stages 1 and 2 to stage 3 as well, with insignificant loss of accuracy. Eq. (40) then becomes:

$$\begin{aligned}
&\frac{N}{N_p}=\left(\frac{16}{\beta^2 c}\left(\frac{A_w}{A_e}\right)^2-\left(2\frac{A_p}{A_e}-1\right)\right)\left[\exp\left(-\frac{\beta c}{4}\frac{A_e}{A_w}\frac{w}{h_w}\right)-1\right]\\
&\qquad+\frac{4}{\beta}\frac{A_w}{A_e}\frac{w}{h_w};\quad \left(stage\,1,2,3:\frac{N}{N_p}<1\right)\\
&\frac{N}{N_p}=1;\quad stage\,4
\end{aligned} \tag{41}$$

The development of the bending moment is calculated from:

$$
\begin{aligned}
&\frac{M}{M_p}=1; \quad \left(stage\,1: \frac{N}{N_p} \le \frac{2A_p}{A_e}-1 \right) \\
&\frac{M}{M_p}=1-\frac{1}{4}\frac{1}{1+2\dfrac{A_t}{A_w}}\left(\frac{A_e}{A_w}\right)^2\left(\frac{N}{N_p}-\left(\frac{2A_p}{A_e}-1\right)\right)^2; \quad \left(stage\,2: \frac{2A_p}{A_e}-1<\frac{N}{N_p}<1-\frac{2A_t}{A_e} \right) \\
&\frac{M}{M_p}=\frac{\dfrac{A_e}{A_w}}{1+2\dfrac{A_t}{A_w}}\left(1-\frac{N}{N_p}\right); \quad \left(stage\,3: 1-\frac{2A_t}{A_e} \le \frac{N}{N_p}<1 \right) \\
&M=0; \quad stage\,4
\end{aligned}
\tag{42}
$$

The resistance versus deformation is plotted in Fig. 9 for stiffened panels with cross section T6 (see *section 5.1*) and various degrees of axial stiffness. When c approaches infinity, the solution converges correctly to the solution for fixed ends in the entire deformation range. For all values of c, when the deformation becomes sufficiently large, the resistance converges to the pure tension solution for fixed ends.

In an actual structure, the stiffness of the structural boundary k could be measured by removing the stiffened panel and applying an inward pulling force. The tangent to the force displacement curve is the required boundary stiffness. To reduce the influence of the adjacent structures during measurement, adjacent stiffened frames should also be removed. From Fig. 9, a non-dimensional stiffness factor c of 1.0 yields quite strong boundaries close to fixed ends. Typical values of c range from 0 to 1 for conditions from no axial fixity to virtually fixed boundaries.

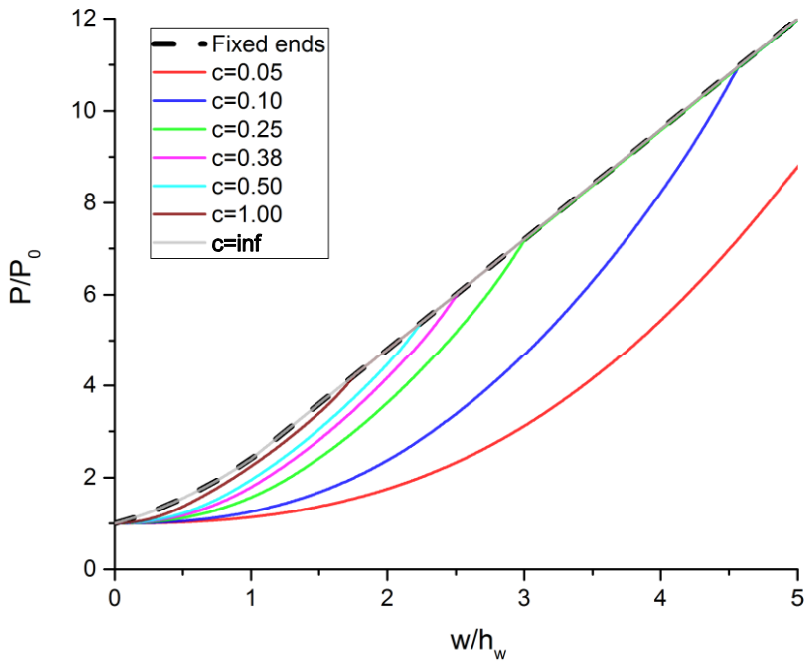

Fig. 9. Resistance-displacement curves for the fixed-end T6 stiffened panel given different translational stiffnesses

4. Comparison with experiments

A few experiments have been carried out on the resistance of stiffened panels subjected to large lateral deflections. Most of the experiments are not directly relevant to the proposed model because the boundaries were fixed in both longitudinal (along the stiffeners) and transverse (perpendicular to the stiffeners) directions, and deformations were significant with respect to the span in both directions. The stiffened panels in such cases cannot be treated as beams. The present model may be further developed to account for the transverse contributions in future work.

Daley and Hermanski [18] conducted an experimental study of single stiffened panel indented laterally by a rigid steel block. Kim [19] reported experimental data of full scale ship grillages subjected to lateral ice indentation. The purposes of the experiments were to check the resistance of ship stiffened panels loaded beyond plastic bending limits. The results from both experiments are used to verify the proposed model.

4.1 Single frame experiments subjected to lateral indentation, by Daley and Hermanski [18]

In the experiment by Daley and Hermanski [18], single frames stiffened with a T stiffener or a flat bar stiffener were loaded at the frame middle span. Dimensions of the frame cross sections are shown in Fig. 10(a) and (b). The frames were 2 meters long, and were held rigidly at the ends. The load was applied through a '102×102 mm' rigid square steel block mounted on the load jack. The experimental setup is shown in Fig. 10(c). Tensile tests were performed to obtain the stress-strain curve. The material curve is shown in Fig. 11 and the yield stress is 340 MPa. The load-

displacement curves predicted by the proposed model are compared to the experimental curves in Fig. 12. For the simplified method, the lateral displacement is adjusted by adding the elastic displacement to the plastic value.

For the flat bar stiffened frame, good agreement is obtained. The frame was loaded to a lateral deflection of 100 mm in the experiment, which is 0.5 times the web height. Tripping was not observed from the experiment (refer Fig. 13, right), and local buckling occurred at the frame ends. For the T stiffened frame, the proposed model captures the initial bending capacity of the frame, but then slightly overestimates the resistance due to tripping of the T stiffener (refer Fig. 13, left). The T stiffener trips over its attached plate at an indenter displacement of 50 mm (including the elastic displacement) accompanied with a force drop. The level of the drop is, however, not significant.

Daley and Hermanski [18] found that T stiffened frames were more susceptible to tripping than flat bar stiffened frames. Two major effects may contribute to tripping of a T stiffened frame. One is that the top flange of the T stiffener is far above the plastic neutral axis (within the attached plate), and is stretched the most. The tension force imposes significant compression on the web, and small deformation induced asymmetry will finally lead to instability and tripping. The other influencing factor of tripping is the web strength. A stiffener web with small web height or large thickness will preserve large capacities to resist compression imposed by the top flange without tripping. Note that the effect of tripping will be limited when the axial membrane forces predominate.

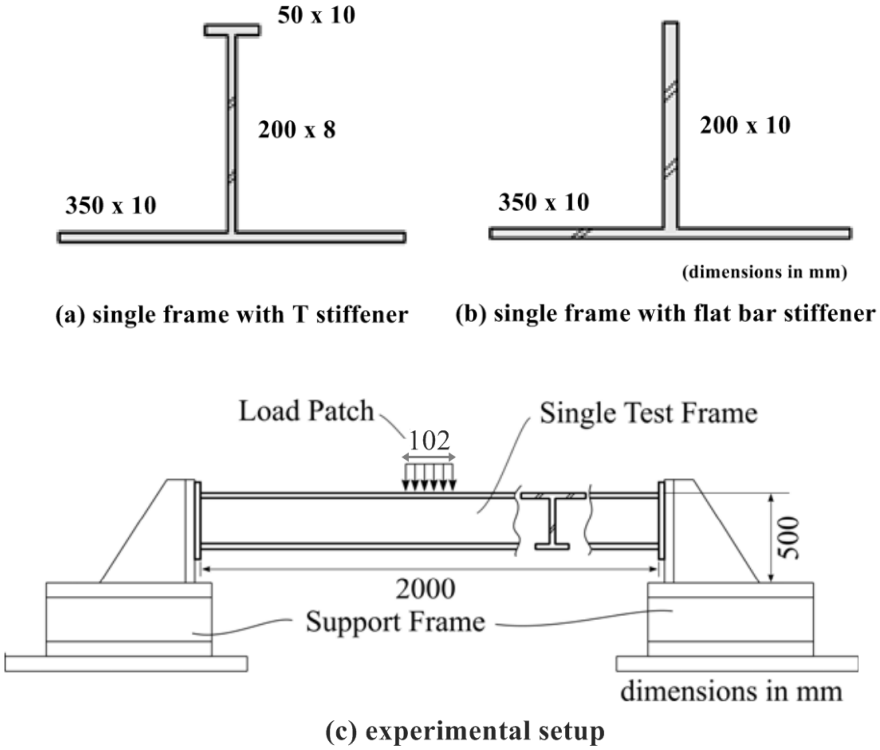

Fig. 10. The setup of the experiment, from Daley and Hermanski [18]

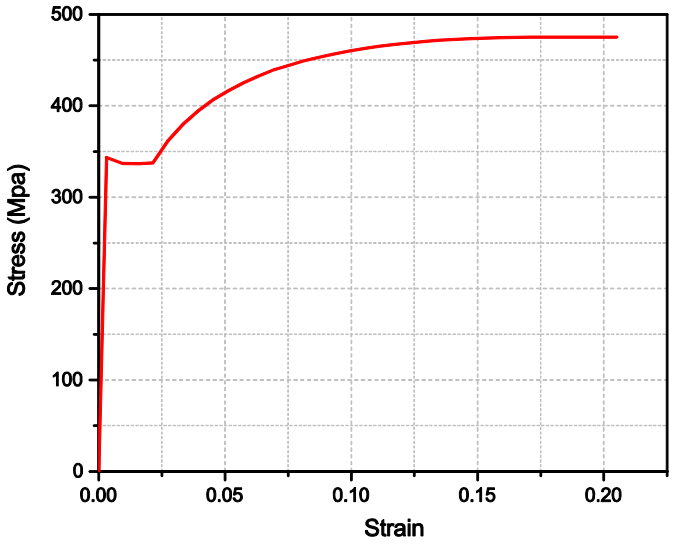

Fig. 11. The measured material stress-strain (engineering) curves from the experiments, Daley and Hermanski [18]

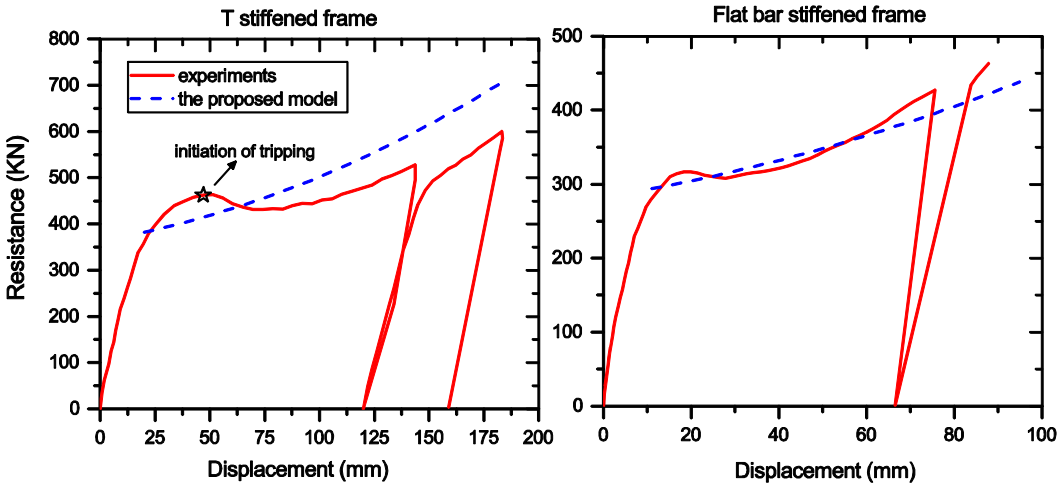

Fig. 12. Force-displacement curves from the experiments and predicted by the proposed model

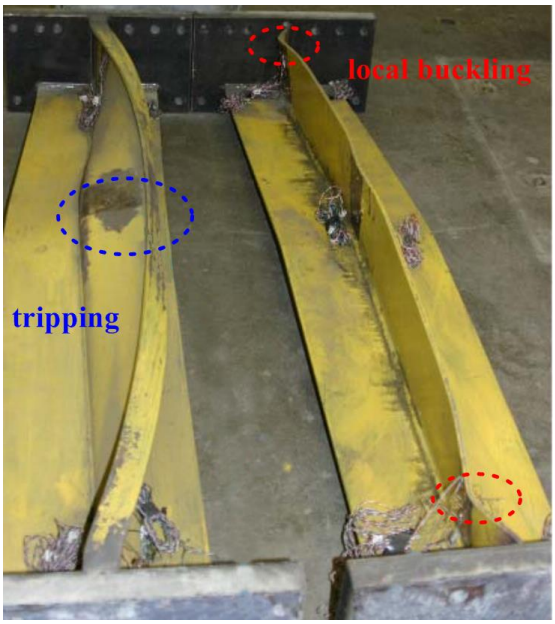

Fig. 13. The deformed frames after the tests, from Daley and Hermanski [18]

4.2 Experiments of full scale ship grillages subjected to ice indentation, from Kim [19]

In the experiments reported by Kim [19], a full scale ship grillage was loaded with a cone shaped ice indenter. The grillage consisted of a plate (6.756 m long and 1.460 m wide), three continuous T stiffeners (web 200 x 8 / flange 75 x 10), two supporting transverse stringers (325 x 18 / 120 x 18) and two heavy side bars (100 x 30). The stringer spacing was 2 m and the stiffener spacing was 350 mm. The stiffeners ran through the stringers and stiffener web plates were supported by the sides of the stringer. The structural dimensions and the experimental setup are shown in Fig. 14. The ends of the longitudinal grillage and the ends of the transverse stringers were held rigidly; refer Fig. 15. The ice indenter was cone-shaped with the bottom diameter of 1000 mm and the cone height of 289 mm; refer Fig. 16(a). The cone inclination angle was 30^{o}. The ship grillage was loaded quasi-statically (0.5 mm/s) at the center (red region in Fig. 14) with a hydraulic ram. Because of the limitation of the ram stroke, the structure was loaded twice to obtain a large indentation.

During the loading process, the contact area increased continuously with the deformation of both the ice and the structure from an initial contact diameter of 50 mm, to a contact diameter of 500 mm at the end of the first loading period and 714 mm at the second period end; refer Fig. 17. It is observed that the two side stiffeners deflected approximately 0.6 times the displacement of the central stiffener at the end of both loading periods.

To apply the proposed simplified model, it is convenient to divide the structure into several part (refer Fig. 14, section A-A), including one central single stiffened frame with the characteristic displacement of the structure, two side stiffened frames with 0.6 times the displacements of the central frame. The rest of the grillage cross section is considered as a sum of the contributions from several rectangular beams with 0.6 times the displacements of the central frame. The governing equations for fixed-end rectangular beams are simple and can be found in Jones [7].

Little deformation was found for the stringers after the experiments. It is therefore reasonable to assume rigid supports at the frame ends.

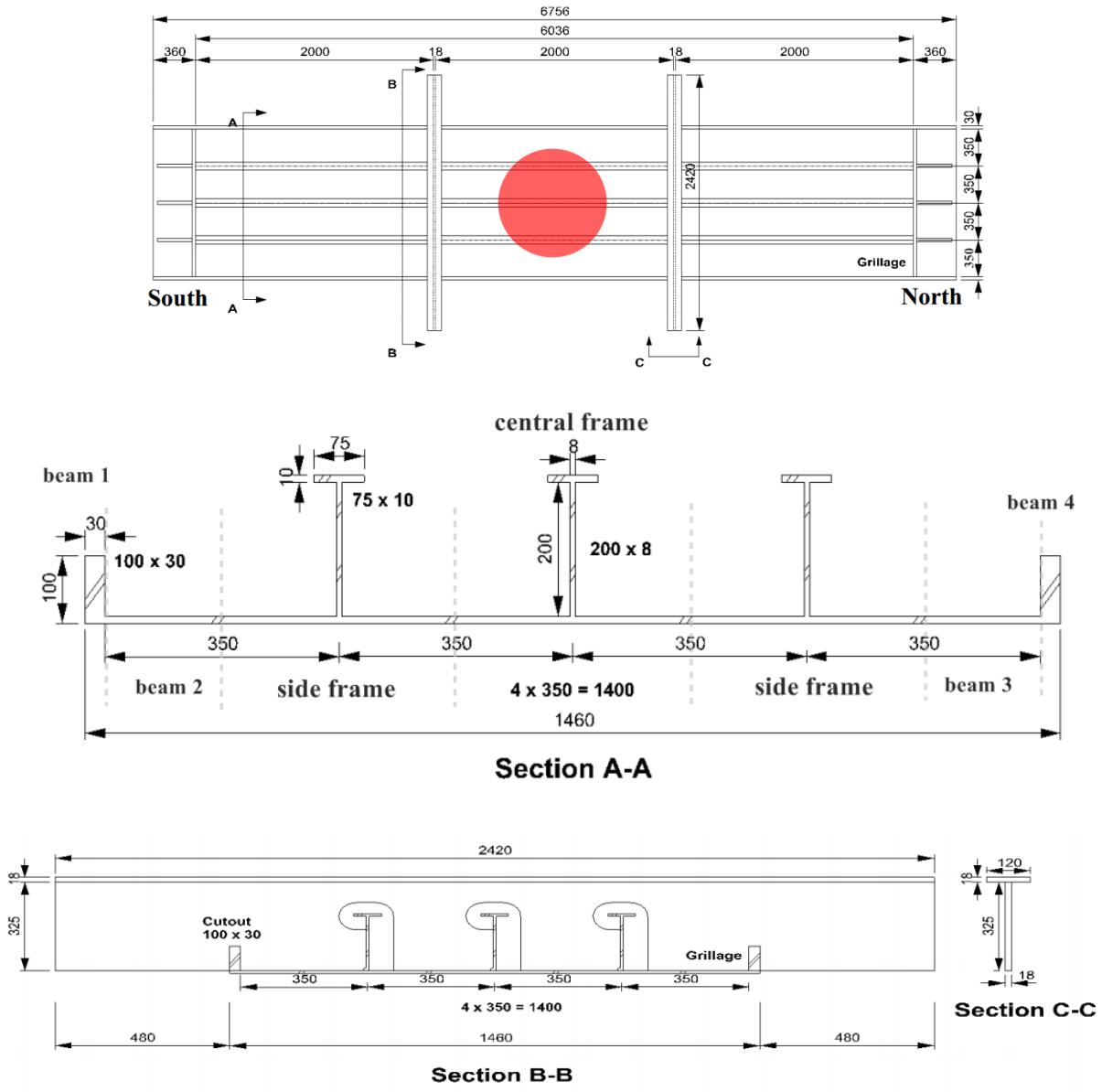

Fig. 14. Dimensions of the ship grillage and the experimental setup, from Kim [19]

(a) fixed at the longitudinal end (b) fixed at ends of transverse stringers

Fig. 15. Boundary conditions of the grillage, from Kim [19]

(a) before test (b) after test

Fig. 16. The ice indenter before and after the test

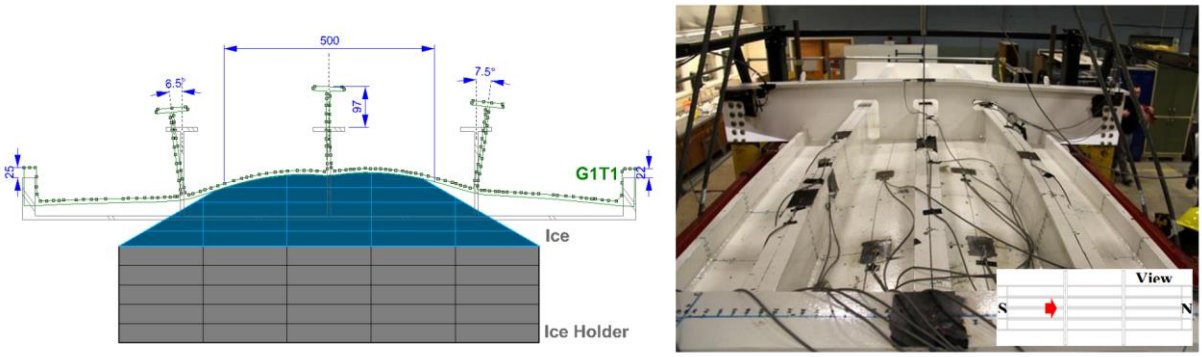

(a) structural deformation after the first loading period

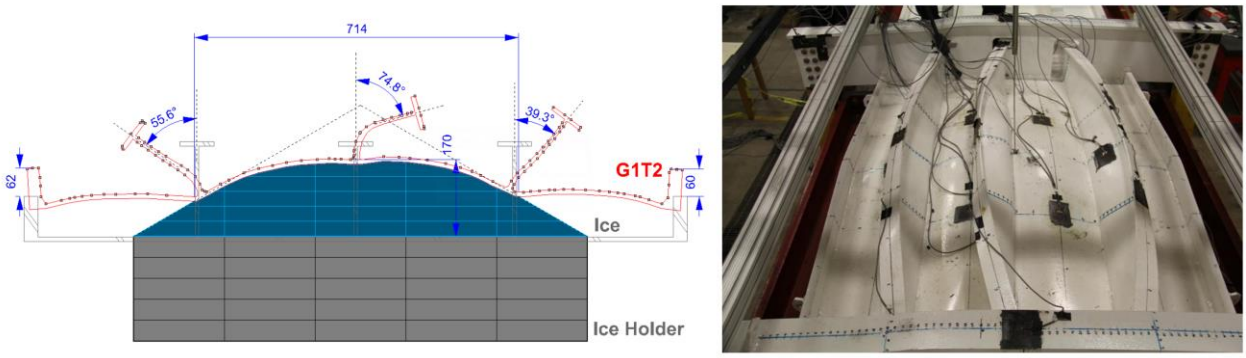

(b) structural deformation after the second loading period

Fig. 17. Deformation of the ship grillage after the first and second loading, from Kim [19]

The stress-strain curve of the steel in the grillage obtained from experiments is shown in Fig. 18, and the yield stress is 410 MPa. The resistance-displacement curves predicted by the proposed model are compared to the experimental curve in Fig. 19. The green, black and blue curves represent the analytical curves for the central frame, the resultant contribution of the central and side frames and the entire grillage, respectively. For the curves by the simplified method, the lateral displacement is adjusted by adding the elastic displacement to the plastic value. Results show that the proposed model predicts well the ultimate strength of the ship grillage regardless of stiffener tripping. The effect of tripping seems limited because tripping occurs at a large panel lateral deflection and membrane forces predominates over bending. Further decrease of bending moment due to tripping leads to insignificant change of the overall resistance.

From the experimental curve, the grillage starts with deformation of the central frame. As lateral indentation continues, the contact area increases with the deformation of both the ice and the structure, and side frames get involved in the deformation. Therefore, there is a gradual change of the force-displacement curve from the initial bending limit of the central frame to the ultimate strength of the entire grillage. The good agreement of experimental and analytical curves at large deformations demonstrates the applicability of the proposed method.

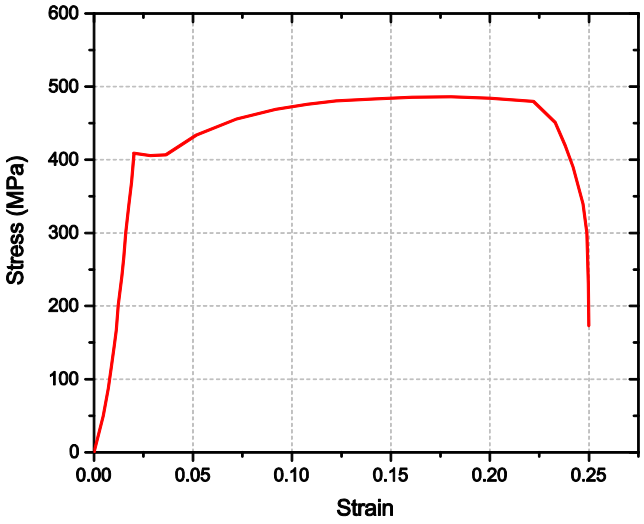

Fig. 18. Material stress-strain curves obtained from tensile tests, Kim [19]

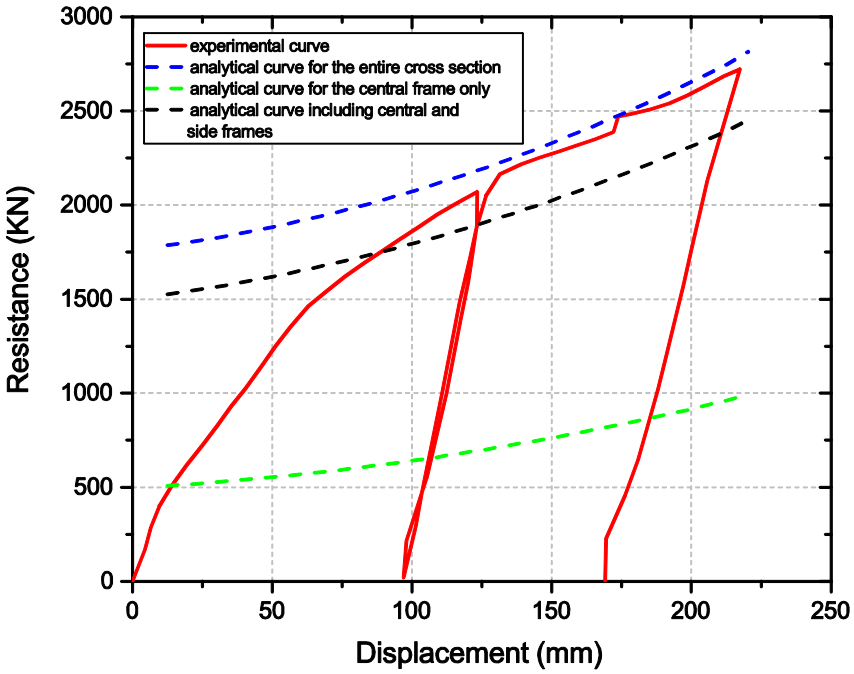

Fig. 19. Force-displacement curves from the experiments and predicted by the proposed model

5. Comparison with nonlinear finite element analysis

Nonlinear finite element analysis (NLFEA), often considered as 'virtual experiments', is used to verify the proposed analytical model comprehensively.

5.1 FE models

Numerical simulations of 5 m long stiffened panels struck by a flat indenter with a constant velocity of 0.2 m/s at mid-span were conducted with the nonlinear finite element code LS-DYNA 971. The selected stiffened panels are long so that all the four deformation stages will exhibit before fracture. The panels were fixed against rotation at both ends and had different degrees of axial flexibilities. Discrete beam elements were used to model axial springs. The panels had different A_p / A_s and A_w / A_t ratios and stiffener area $A_s = A_w + A_t$; refer to Table 1. The geometry was modeled with four-node Belytschko-Lin-Tsay shell elements with five integration points through the thickness. At least six elements were used over the stiffener web and the top flange such that possible tripping and local buckling could be well captured. The typical FE mesh is shown in Fig. 20. A friction coefficient of 0.3 was employed.

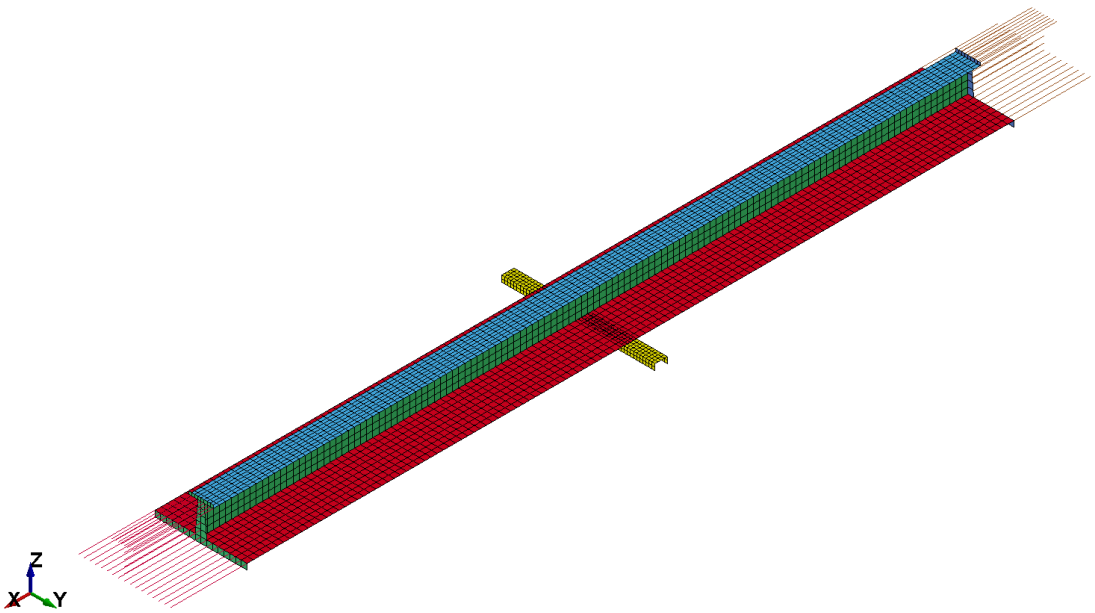

Fig. 20. An example of a stiffened panel model

Two different materials were used, with stress-strain curves plotted in Fig. 21. Because the simplified method is based on a rigid perfectly plastic material, material 1 had small, linear hardening. Moderate hardening is needed to avoid excessive concentrations of plastic strains in narrow regions, which would yield imprecise response predictions. Material 2 had a more realistic hardening, which was represented with the power law model with a yield plateau. The material properties are given in Table 2. Fracture was not considered for material 1, whereas the Rice-Tracey-Cockcroft-Latham (RTCL) damage criterion [24] was used for material 2.

Table 1. Dimensions of different stiffened panel cross sections (Unit: mm)

Cross section type	A_p/A_s	A_w/A_t	A_p	A_w	A_t
T1	1	1	600 x 8	240 x 10	200 x 12
T2	1	2	600 x 8	200 x 16	160 x 10
T3	1	3	600 x 8	300 x 12	100 x 12
T4	2	1	600 x 8	150 x 8	120 x 10

T5	2	2	600 x 8	160 x 10	100 x 8
T6	2	3	600 x 8	180 x 10	100 x 6
T7	3	1	600 x 8	160 x 5	100 x 8
T8	3	3	600 x 8	120 x 10	50 x 8

Table 2. Material properties for stiffened panels

Material	*Hardening type*	σ_y *(MPa)*	*E (GPa)*	*K (MPa)*	*N*	E_t *(MPa)*	$\varepsilon_{plateau}$
Material 1	Linear	355	207	-	-	400	-
Material 2	Power law	355	207	780	0.22	-	0.026

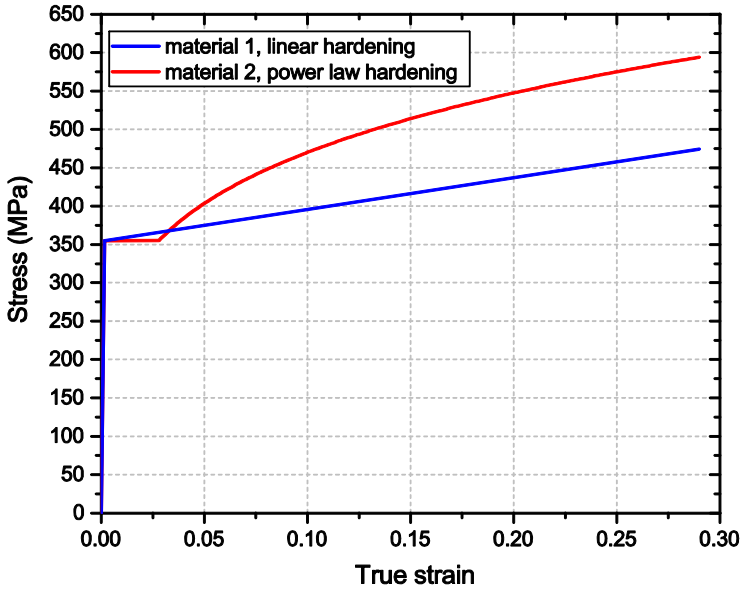

Fig. 21. Stress-strain curves for the two materials

5.2 Resistance with axially fixed ends

A 50 mm wide rigid indenter was crushed into fixed-end stiffened panels with eight different cross sections as defined in Table 1. The obtained resistance-displacement curves from LS-DYNA are compared with predictions by the simplified method in Figs. 22 and 23. For the simplified method, the lateral displacement is adjusted by adding the elastic displacement to the plastic value.

The results agree well. Good accuracy is found especially when the soft hardening material 1 is used. When material 2 is used, the simplified method tends to underestimate the resistance as the lateral deflection increases, and the difference is especially obvious in the pure tension stage. This is because, in the pure tension stage 4 where plastic hardening is significant, the yield stress σ_y is still used in the simplified model instead of the flow stress σ_{flow}. Thus, there is a slope difference of σ_{flow} / σ_y between the predicted and simulated resistance curves.

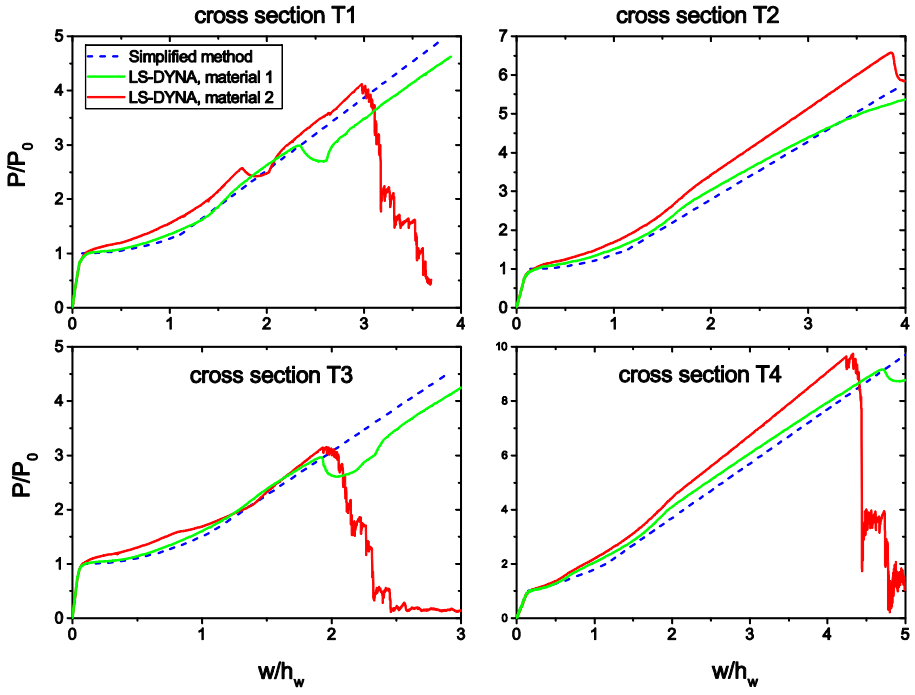

Fig. 22. Nondimensional resistance curves for fixed-end stiffened panels with cross section T1-T4

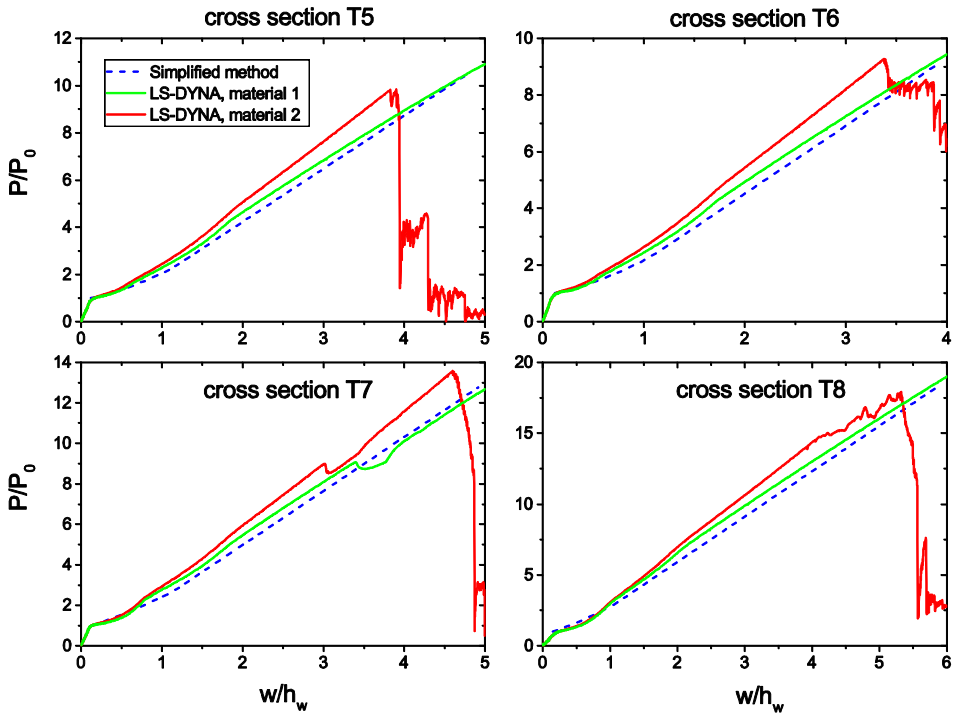

Fig. 23. Nondimensional resistance curves for fixed-end stiffened panels with cross section T5-T8

Local buckling of stiffeners may occur during deformation accompanied by a force drop. An example of a buckled stiffened panel is shown in Fig. 24. Stiffener buckling has limited influence on the prediction accuracy of the proposed simplified model because it mainly reduces the bending moment M and has little influence on the membrane force N. Buckling usually occurs after a displacement of several times the stiffener web height h_w. The stiffened panel develops quickly into the full tension stage, with little bending moment remaining after a displacement of h_w, and the resistance is thus only slightly influenced by stiffener buckling. Fracture occurs early for cases with small L / h_w ratios.

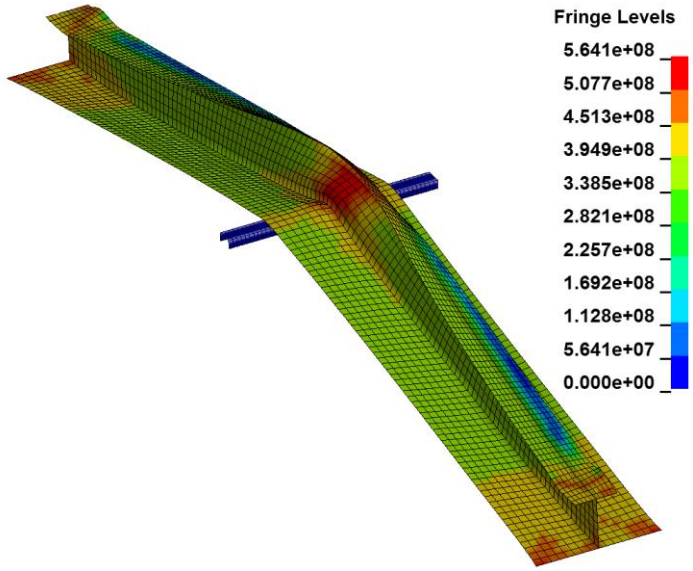

Fig. 24. Local buckling of a stiffened panel

5.3 Resistance with finite translational stiffness

Resistance curves for stiffened panels with finite translational stiffness, obtained with the simplified method and numerical simulations using material 2, are compared in Figs. 25, 26 and 27 for fixed rotation conditions at the ends and in Fig. 28 for free rotation conditions at the ends.

The results agree well, notably when the axial stiffness is moderate. In the pure tension stage, the simplified model has a smaller slope due to missing hardening. The small force drops in the numerical simulation curves are due to local buckling. The influence of stiffener local buckling on the prediction accuracy is limited.

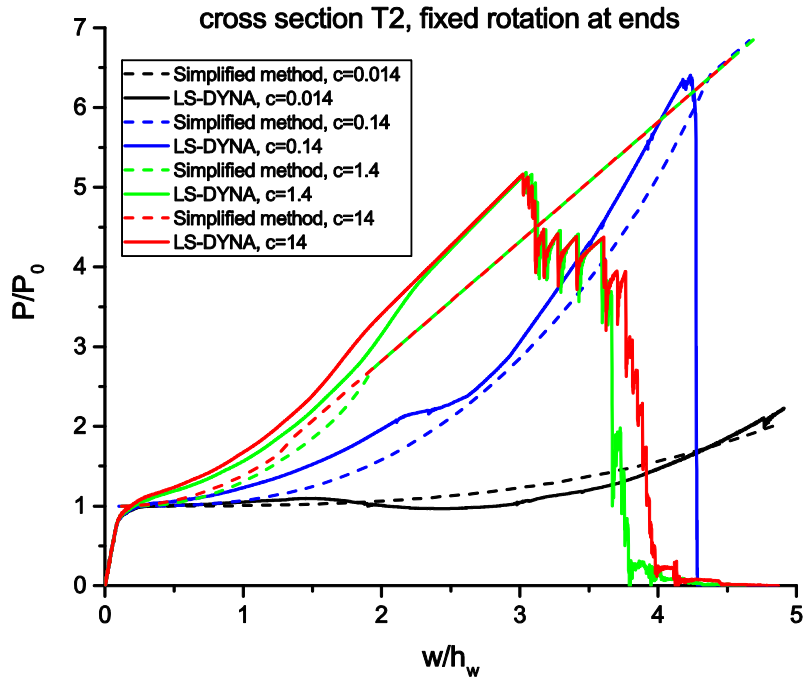

Fig. 25. Nondimensional resistance for the T2 stiffened panels with fixed rotation conditions at the ends

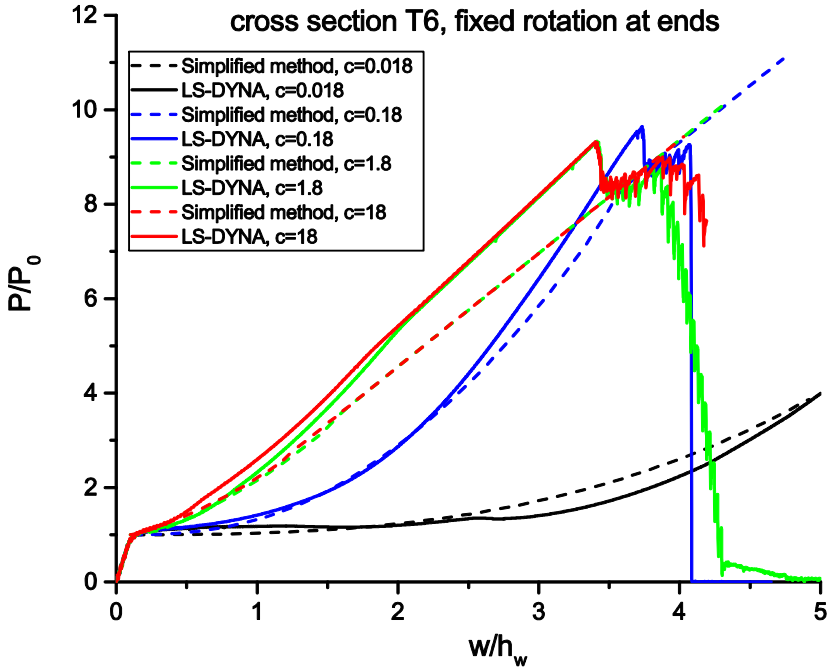

Fig. 26. Nondimensional resistance for the T6 stiffened panels with fixed rotation conditions at the ends

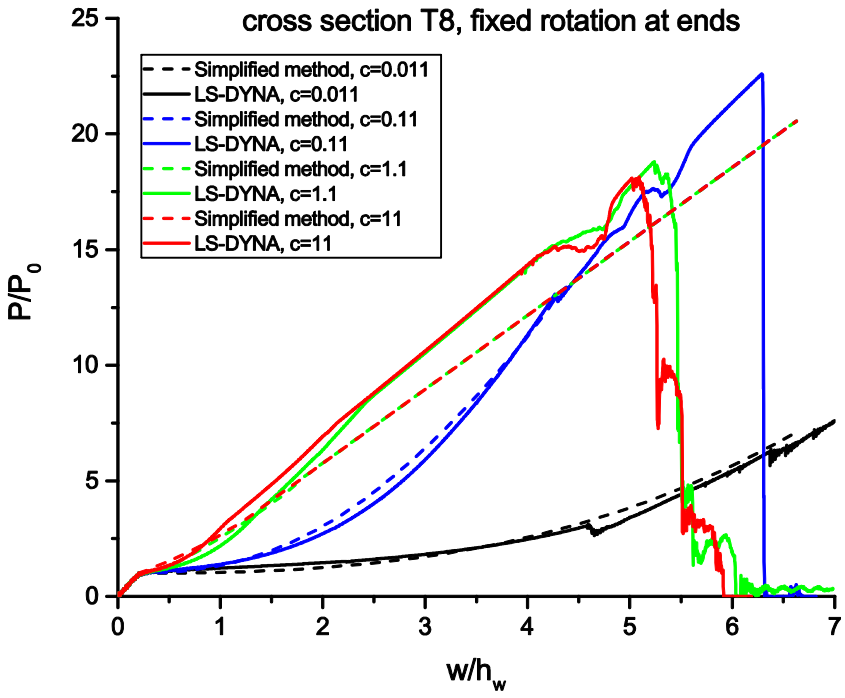

Fig. 27. Nondimensional resistance for the T8 stiffened panels with fixed rotation conditions at the ends

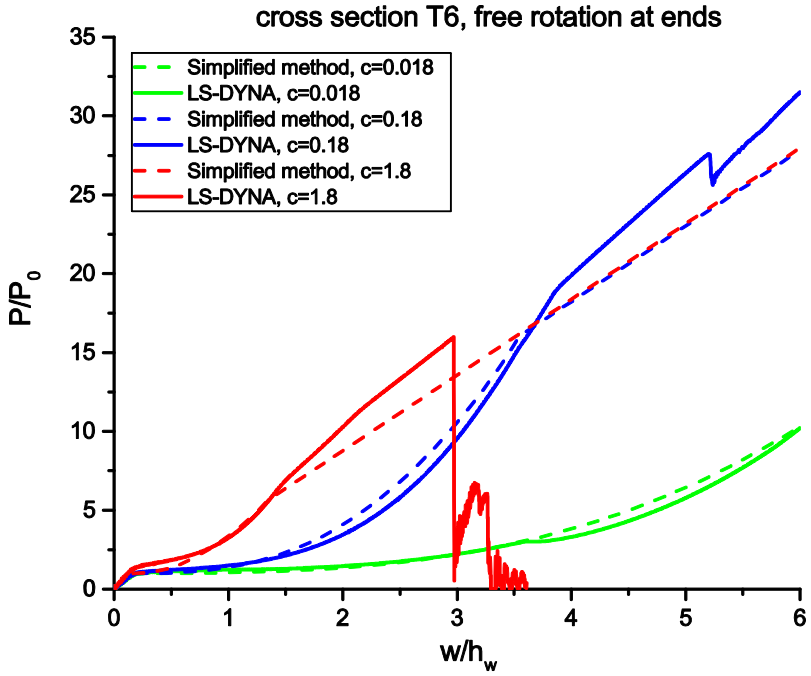

Fig. 28. Nondimensional resistance for the T6 stiffened panels with free rotation conditions at the ends

A simple expression for tension fracture prediction in yield hinges is given in the NORSOK N004 standard [4]. In Table 3, the corresponding critical deflections are compared with the results of the numerical simulation presented in Figs. 25-27. Reasonable prediction is obtained. The NORSOK criterion for rupture is conservative for stiffened panels with the T2 and T6 profiles, but the fracture deflection is overestimated to some extent for the T8 profile. Note that the RTCL criterion is used in numerical simulations, which does not necessarily represent the "true" behavior.

Table 3. Normalized critical fracture deflections for stiffened panels with different cross sections

	Profile T2				Profile T6				Profile T8			
c-factor	0.014	0.14	1.4	14	0.018	0.18	1.8	18	0.011	0.11	1.1	11
Predicted w_{cri}/h_w	3.8	3.6	3.2	2.7	4.7	4.4	3.7	3.2	10.7	9.6	7.4	5.9
Simulated w_{cri}/h_w	>5.0	4.3	3.3	3.3	>5.2	4.2	3.8	3.8	>7.0	6.4	5.6	5.4

5.4 Resistance of stiffened plates with non-central and patch loads

The lateral deformation resistance of stiffened panels for various indenter widths B, impact positions α (refer to Fig. 8), and uneven axial stiffness is simulated, and material 2 is used.

The resistance curves for small axial stiffness and varying patch load, shown in Fig. 29, generally agree well with numerical simulations. A major cause for the differences is the effect of hardening. The results confirm that a "hard" patch load reduces the effective beam length and thus increases the resistance. Fig. 30 shows the resistance for uneven axial stiffness, i.e., $k_1 \neq k_2$. Disregarding hardening, the agreement is quite good. The resistance plots for non-central impacts, shown in Fig. 31, demonstrate again that the simplified method yields good results in view of the hardening effect. The resistance is larger for non-central impacts, but at the same time, fracture occurs earlier due to increased shear forces at the closest support.

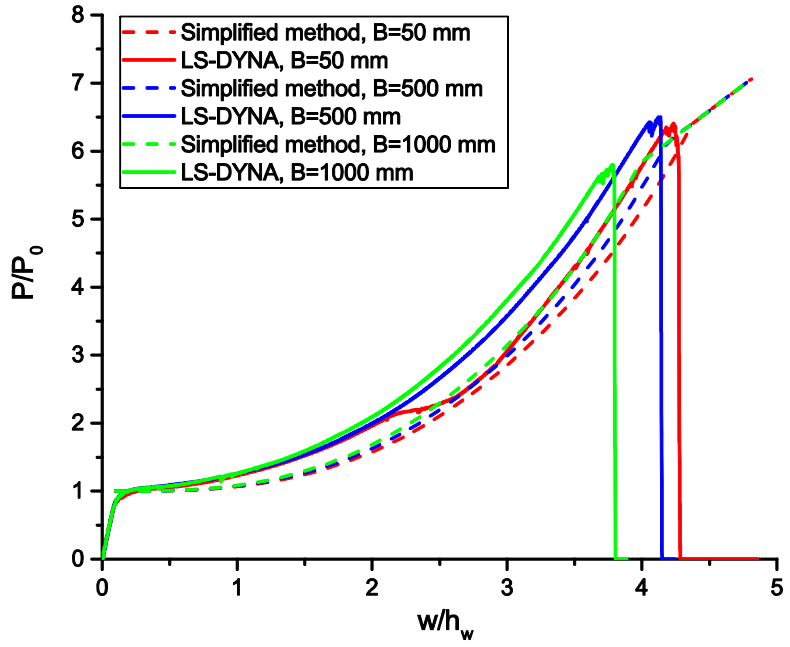

Fig. 29. Nondimensional resistance for the T2 stiffened panel with α=0.5, c=0.07 and various contact lengths

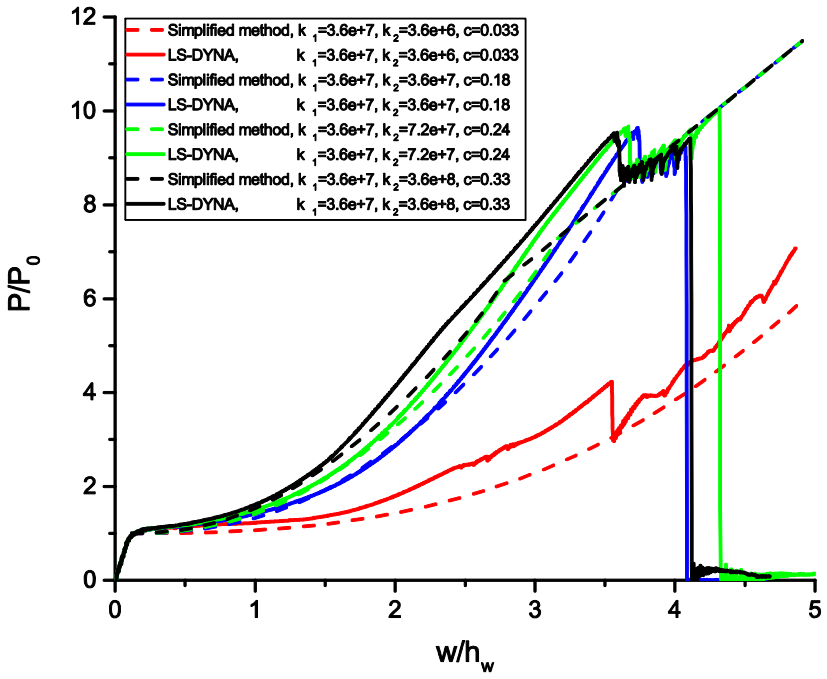

Fig. 30. Nondimensional resistance for the T6 stiffened panel with α=0.5, B=50 mm and uneven axial stiffness

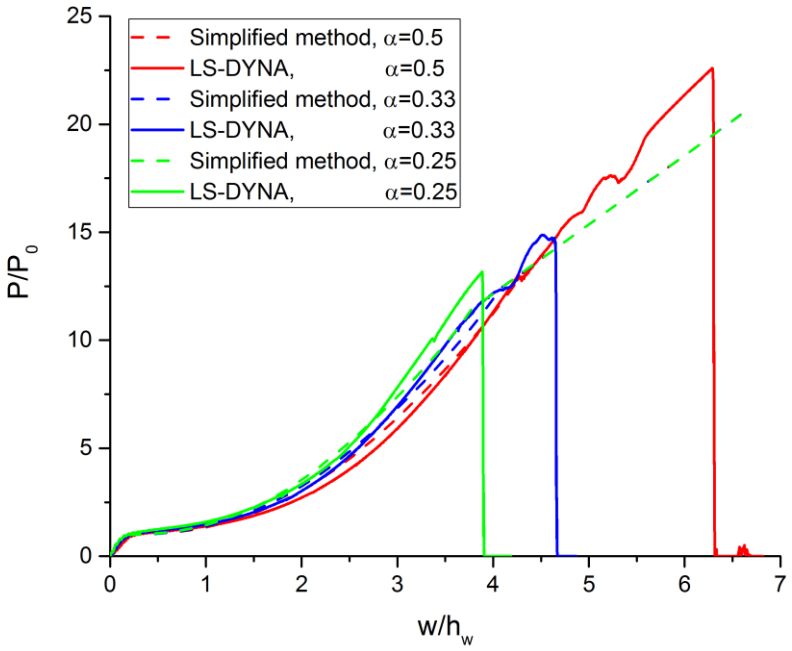

Fig. 31. Nondimensional resistance for the T8 stiffened panel with B=50 mm and different α. The stiffness at both ends is 4.3×10^7 N/m, yielding c = 0.11, 0.12 and 0.14 for α=0.5, 0.33 and 0.25.

5.5 Resistance with uniformly distributed loads

The ends of the panel are clamped against rotations and fixed against inward motion, i.e., c= infinity. The force displacement curves for the four different cross sections in Fig. 32 show that the simplified method captures the response quite well, but the capacity is somewhat underestimated. This may be because the assumption of using $0.5pL$ to approximate uniform distributed loads is derived based on the similarity of plastic bending collapse, but is not exactly satisfied in the membrane stage. The neglect of the material hardening may also contribute to the difference.

It is observed that fracture occurs much earlier in cases with uniformly distributed pressure loads compared to those with point loads. This is because uniform loading gives much reduced central deflections if the same total force is applied, but the shear forces at the supports are equal for both scenarios being $0.5pL$ at each end (see Fig. 33). Based on the plastic hinge theory assuming a linear displacement field, for the same lateral deflection, the shear force at the support with uniform loading is twice the force with point loading, and fracture thus occurs early at the support under the combined action of bending, tension and the significant shear forces.

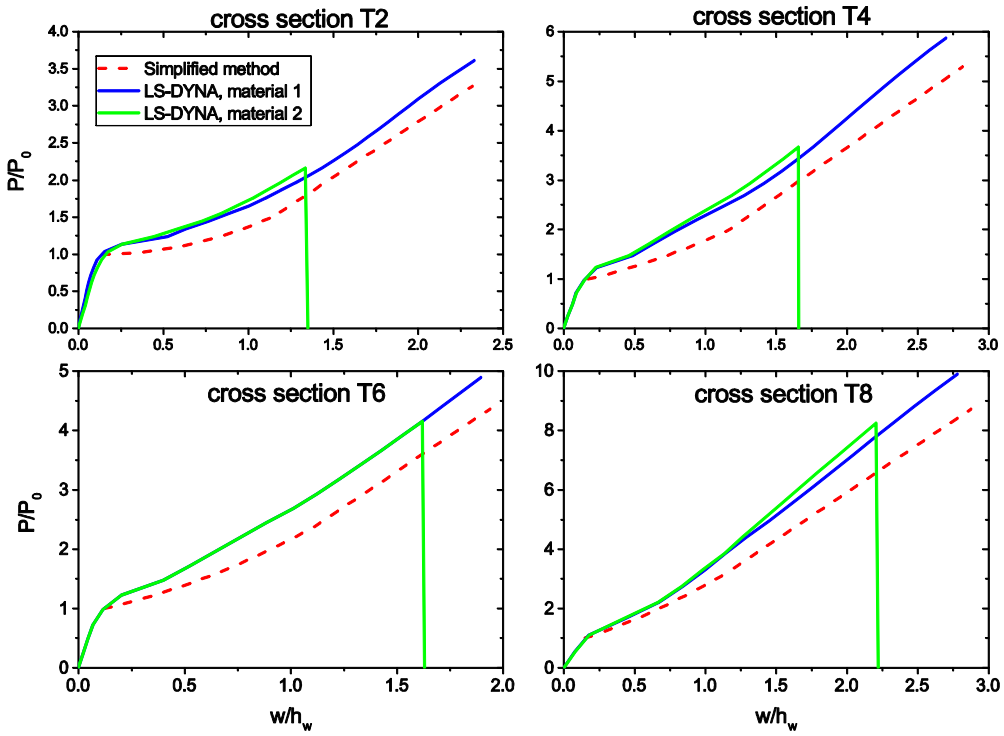

Fig. 32. Resistance curves for stiffened panels subjected to uniformly distributed pressure loads

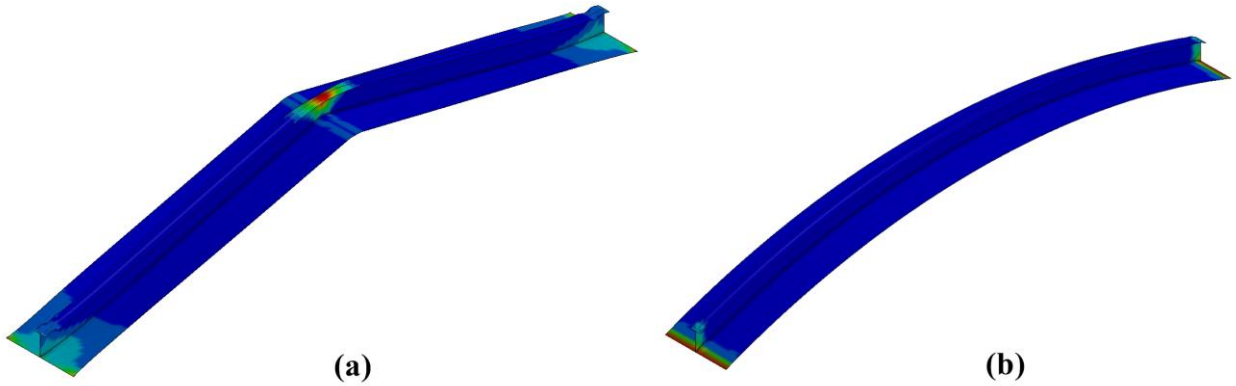

Fig. 33. Strain distribution of deformed stiffened panels under (a) point loads and (b) uniform pressure loads

5.6 The effect of inertia forces on the resistance

The influence of inertia forces is studied for the T6 stiffened panel by varying the indenter speed. Material 1 is used, and any strain rate effects are not considered. The ends are fixed against inward motion. Fig. 34 shows that the resistance oscillates in the initial stages, noticeably for the highest impact speed. The effect increases with increasing impact speed. The force tends to become stable as the indentation increases. The simplified method appears to be quite accurate as far as the average resistance is concerned, and the total dissipated energy is close to the static solution despite force oscillations.

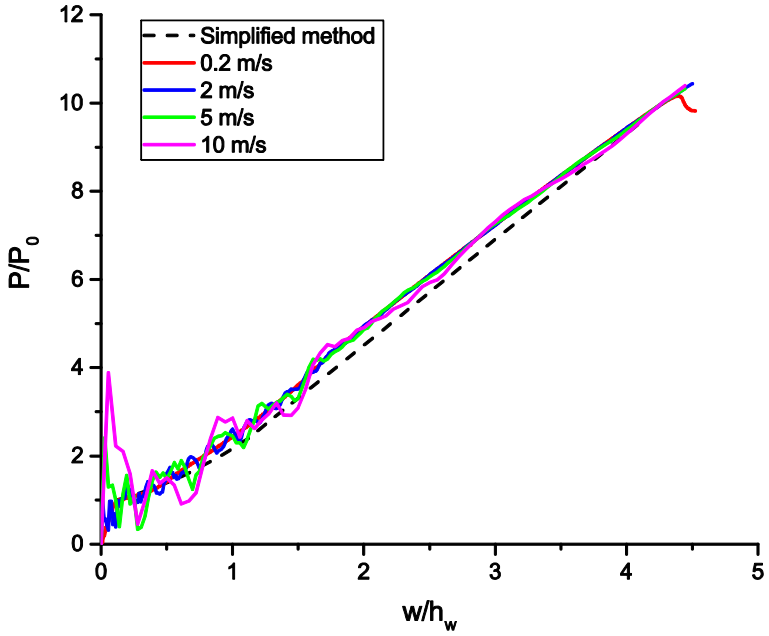

Fig. 34. Resistance curves of the T6 stiffened panel for different impact velocities

5.7 The influence of transverse shear on the resistance

For a stiffened panel with clamped boundaries, the static transverse shear force transferred to the support in the plastic bending phase is $Q_s = 4M_p / L$. The shear force is assumed to be carried by the stiffener web only, and the yield force in pure shear is $Q_0 = \frac{1}{\sqrt{3}}\sigma_0 A_w$. The shear force-yield shear force ratio becomes:

$$\frac{Q_s}{Q_0} = \frac{2\sqrt{3}(A_w + 2A_t)}{A_w}\frac{1}{L/h_w} \le 1 \tag{43}$$

The shear force has a relatively small effect on the plastic bending moment as long as the shear force ratio does not approach close to unity, i.e., for panels with large length/web height ratios. For cross section T2, the ratio becomes $\frac{Q_s}{Q_0} = \frac{4\sqrt{3}}{L/h_w}$. The effect of shear force is studied by varying the beam length such that L/h_w equals 12, 10, 8 and 5, giving Q_s/Q_0 being 0.58, 0.69, 0.87 and 1.38. The resistance curves are plotted in Fig 35.

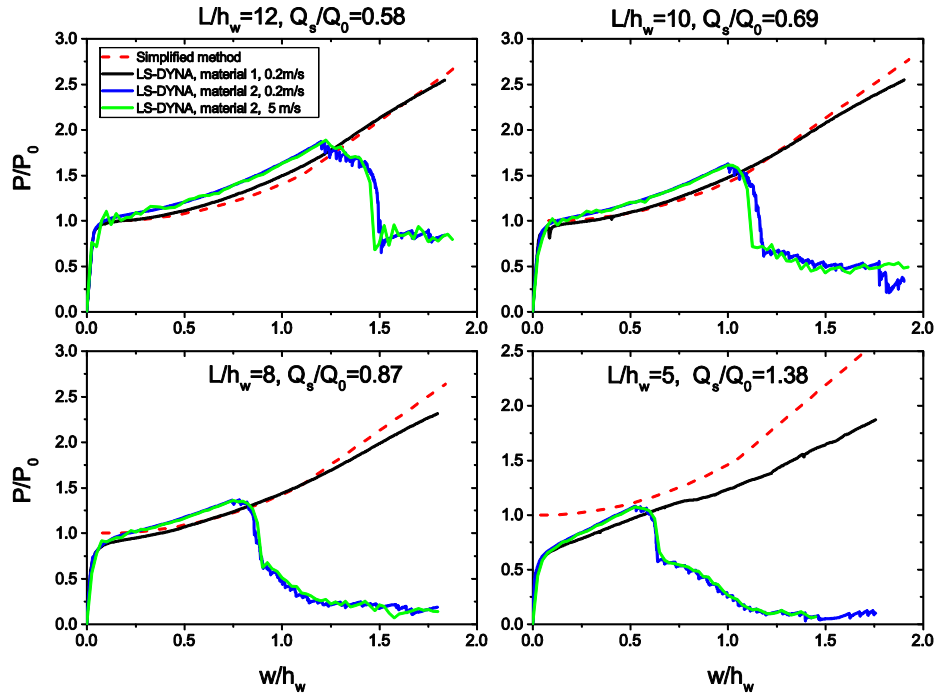

Fig. 35. Nondimensional resistance-deformation curves for L/h_w=12, 10, 8 and 5

For cases with $L/h_w = 12$ and 10, the simplified model is in good agreement with numerical simulations. When $L/h_w = 8$, i.e., when the shear force is 87% of the yield shear force, there is a small effect from the shear force on the initial collapse load. When $L/h_w = 5$, the web yields in shear, the cross section cannot develop the fully plastic bending moment, and the collapse load is reduced. Material 2 provides a somewhat larger resistance in all cases with stronger hardening. The resistance curves for speeds of 0.2 m/s and 5 m/s are virtually identical and demonstrate that the inertia forces play a small role in this velocity range. The shorter the panel becomes, the earlier the predicted fracture is with the RTCL criterion.

5.8 Panels stiffened with L-profiles

Asymmetric stiffeners, such as L-profiles, will be more susceptible to warping or tripping, which will reduce the load carrying capacity. Three different L-profiles were investigated. The profiles 'L1', 'L2' and 'L6', as defined in Table 4, have the same plate flange, web and top flange areas as cross sections 'T1', 'T2' and 'T6'. The width and speed of the indenter are as in the base cases: 50 mm and 0.2 m/s. Material 1 was used. The effect of a bracket at the mid-section to prevent tripping was also studied; refer to Fig. 36.

Table 4. Stiffened panel cross sections with L-profile stiffeners (Unit: mm)

Stiffener type	A_p/A_s	A_w/A_t	A_p	A_w	A_t
Type L1	1	1	600×8	240×10	80×30
Type L2	1	2	600×8	200×16	80×20

Type L6	2	3	600×8	180×10	60×10

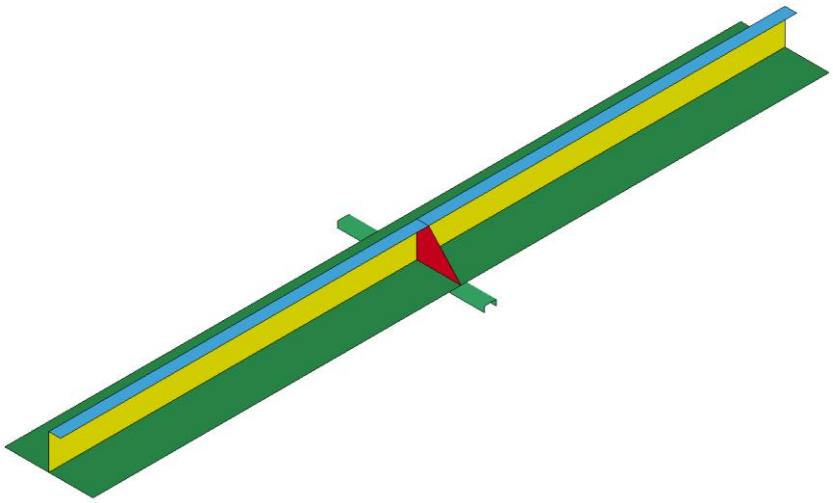

Fig. 36. Impact scenario of a stiffened panel with L-profile stiffeners and a middle bracket

Resistance-deformation curves are plotted in Fig. 37. Stiffener L1 has a large top flange/web area ratio, and tripping causes a noticeable reduction in the resistance. With the mid-span bracket, this is ameliorated, and the simplified method is in good agreement with the simulations. The tripping effect is not observed for stiffened panels with 'L2' and 'L6' stiffeners, which have a large web - top flange area ratio. The web has sufficient bending strength to counteract the asymmetrical bending stresses of the top flange. Tripping occurs at a late stage and has limited influence on the resistance.

When the beam length is reduced to 2.5 m, the panel with 'L2' stiffeners and no bracket experiences tripping early, and the resistance is moderately reduced. When the middle bracket is modeled, tripping and buckling are much delayed, and the simplified method is well applied.

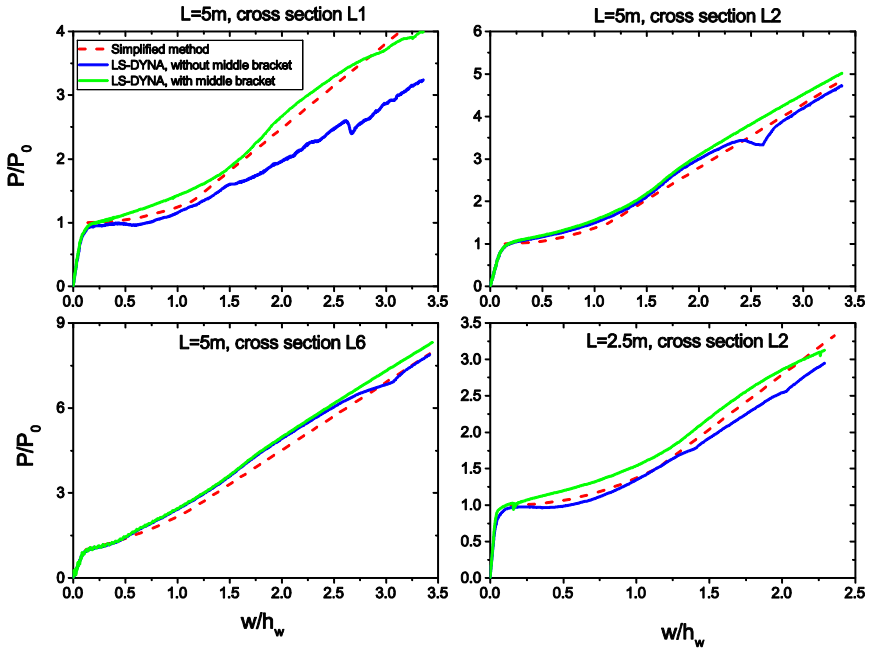

Fig. 37. Nondimensional resistance curves for stiffened plates with L-profile stiffeners

6. Application to structural damage prediction in accidental actions

The proposed formulation provides a useful tool for quick assessment of the structural response of stiffened panels subjected to abnormal or accidental loads such as ship collisions, dropped objects, explosions, slamming, hydrostatic pressure and ice actions. The expressions may also be used in combination with the Monte Carlo method for structural reliability assessments.

In the analysis of ship collisions and dropped objects, the problem is often decoupled into *external dynamics* and *internal mechanics*. External dynamics deal with global motions of the striking and struck bodies before, during and after collisions, and predicts the demand for structural energy dissipation. The commonly used external dynamic models are the 3DOF model by Pedersen and Zhang [25] and the 6DOF model by Liu and Amdahl [26]. The inputs of the external dynamic models are the masses and moments of inertia, the relative positions and the velocities of the striking and struck objects before impact, while the outputs are the velocities after the collision and the dissipation energy. This energy should be dissipated through structural deformations in the analysis of *internal mechanics*. The maximum deformation of the stiffened panel is obtained when the area under the force-displacement curve with the proposed model meets the demand for energy dissipation estimated in the *external dynamics*.

For stiffened panels subjected to transient impulsive loads, e.g. explosions and violent water slamming, a practical analysis method is to use the Single Degree Of Freedom (SDOF) analogy suggested by Biggs [27]. The approach is also adopted in DNV RP C204 [3]. The equivalent system is selected so that the deflection of the SDOF system is the same as that for some representative point on the structure, e.g. the midspan of a beam. It is convenient to assume that

the structure exposed to the dynamic pressure pulse ultimately attains a deformed configuration comparable to the static deformation pattern. Using the static deformation pattern as displacement shape function, i.e.

$$w(x,t) = \phi(x)\, y(t) \tag{44}$$

where $w(x,t)$ is the structural displacement at any point of the structure at any time, $\phi(x)$ is the displacement shape function and $y(t)$ is the displacement of the characteristic point with time.

The dynamic equations of equilibrium can be transformed into an equivalent SDOF system:

$$\bar{m}\ddot{y} + \bar{k}\dot{y} = \bar{f}(t) \tag{45}$$

The generalized mass: $$\bar{m} = \int_l m\phi(x)^2 dx + \sum_i M_i \phi_i^2 \tag{46}$$

The generalized load: $$\bar{f} = \int_l q(t)\phi(x) dx + \sum_i F_i \phi_i \tag{47}$$

where, m is the distributed mass, M_i is the i_{th} concentrated mass, q is the distributed pressure, F_i is the i_{th} concentrated load and $\phi_i = \phi(x = x_i)$.

The equivalent stiffness of the system $\bar{k}$ is the tangent of the resistance-displacement curve, where the resistance equals to total load acting on the structures given the load distribution and magnitude and the displacement is the deflection of the characteristic node. $\bar{k}$ can be obtained from the resistance-displacement curve by the proposed model, but some modifications are necessary to account for the load distribution according to the definition. When $\bar{m}, \bar{k}, \bar{f}(t)$ are known, the SDOF system can be solved analytically or numerically, and the maximum deformation of the stiffened panel can be readily found. For the present case of stiffened panels, it may be convenient to simplify the response curves into three linear stages with stiffnesses of k_1, k_2, k_3 as shown in Fig. 38, where y_{el} is the displacement at the end of the initial linear resistance domain and R_{el} represents the maximum resistance of the structure due to bending. k_1 is determined by the elastic bending stiffness of the panel, while k_2 and k_3 should be determined from the proposed equations.

If k_2 is assumed to be zero and the load acting on the structures can be approximated by a triangular load with maximum value $F_{\max}$ and duration t_d, the maximum deflection of the SDOF system $y_{\max} / y_{el}$ can be directly read from the curve provided by DNV RP C204 [3] as shown in Fig. 39. T is the eigenperiod of the structure in the initial linear resistance domain given by:

$$T = 2\pi\sqrt{\frac{\bar{m}}{\bar{k}}} \tag{48}$$

In Fig. 39, the solid lines were provided by Biggs [27] and represented the response of the SDOF system for the linear elastic-perfectly plastic bending behavior without consideration of the membrane effect. The dashed and dotted lines were developed in the DNV RP C204 [3] to account for the membrane effects with different k_3 stiffness.

From Fig. 39, the maximum structural deflection depends on the duration of the load impulse versus the structural natural period (t_d / T), the maximum bending resistance versus the maximum load ($R_{el} / F_{\max}$) and the structural stiffness. Depending on the t_d / T ratio, the response of a structural component may be classified into three categories: impulsive domain ($t_d / T < 0.3$), dynamic domain ($0.3 < t_d / T < 3$) and quasi-static domain ($t_d / T > 3$). For stiffened panels in the quasi-static domain and slow loading rate, the proposed formulations can be directly applied. For other cases, the SDOF analogy in combination with the proposed static resistance formulation should be used, which simplifies the problem significantly but still provides reasonable accuracy for structural design.

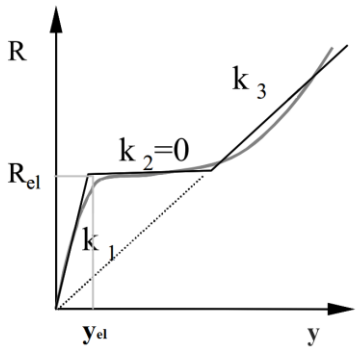

Fig. 38. Representation of the response curve of stiffened panels by an equivalent tri-linear system

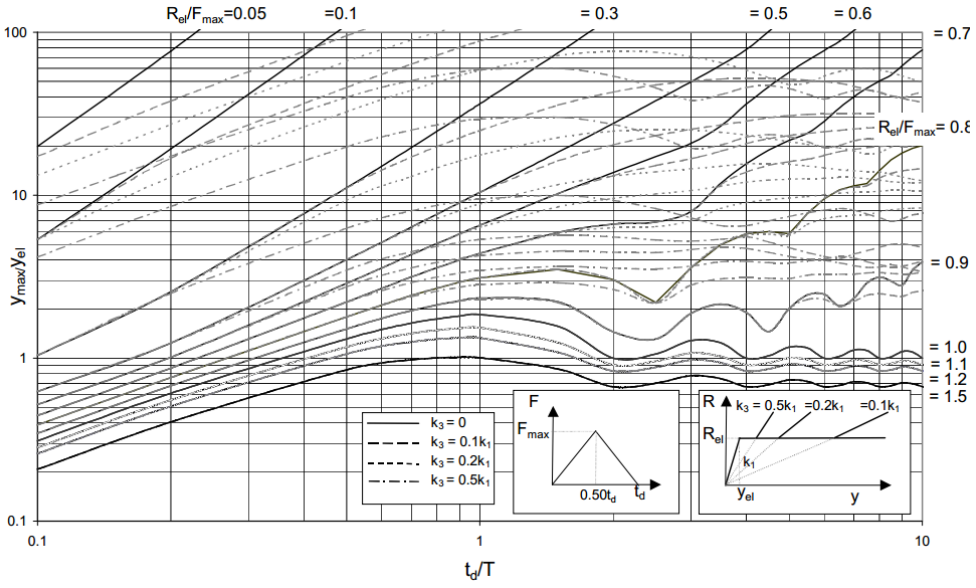

Fig. 39. Dynamic response of a SDOF system to a triangular load (rise time=0.50t_d), from DNV RP C204 [3]

7. Conclusions

Plastic methods have been used to derive a simplified formulation for the large deformation resistance of stiffened panels subjected to concentrated loads, uniformly distributed loads or patch loads. The panels may be simply supported or clamped against rotations at the ends, with various degrees of restraints against inward motion. Experiments and nonlinear finite element analysis with LS-DYNA were used to verify the formulations.

Comparison with the results of experiments and numerical simulations showed that the simplified formulation is capable of predicting the large deformation resistance with high accuracy, provided that the profile is compact and not subjected to tripping at the early stage of deformation or to very high utilization of the web in shear.

Care should be exercised in using the formulations for very asymmetric profiles, which could be subjected to tripping depending on the strength of the web. A tripping bracket at mid-span was found to ameliorate the situation in these cases. The simple method is based on the assumption of a perfectly plastic material, so it underestimates the capacity of stiffened plating with realistic materials considering hardening. Static resistance curves were found to apply very well for average resistance with impact speeds up to 5 m/s. For stiffened panels subjected to highly dynamic or transient impulsive loads, the SDOF analogy can be used in combination with the proposed static resistance curve.

The method may be a useful tool for quick assessment of the resistance of stiffened panels subjected to abnormal/accidental loads, such as ship collisions, dropped objects, explosions, slamming and ice loads.

Acknowledgments

This work has been funded by the Research Council of Norway (NFR) through the Centers of Excellence funding scheme, project AMOS (Grant number 223254) at the Norwegian University of Science and Technology (NTNU). This support is gratefully acknowledged by the authors.

References

[1] Sha Y, Hao H. Nonlinear finite element analysis of barge collision with a single bridge pier. Engineering Structures. 2012;41:63-76.
[2] Sha Y, Hao H. Laboratory tests and numerical simulations of barge impact on circular reinforced concrete piers. Engineering structures. 2013;46:593-605.
[3] DNV-RP-C204. Recommended practice DNV-RP-C204. DET NORSKE VERITAS. 2010.
[4] DNV. NORSOK Standard N004. Design of steel structures, Appendix A, design against accidental actions. Det Norske Veritas 2004. 2004.
[5] Wierzbicki T, Abramowicz W. On the crushing mechanics of thin-walled structures. Journal of Applied mechanics. 1983;50:727-34.
[6] Amdahl J. Energy absorption in ship-platform impacts. Doctoral Thesis, Norwegian Institute of technology1983.
[7] Jones N. Structural impact. Cambridge university press; 2011.
[8] Yu Z, Hu Z, Amdahl J, Liu Y. Investigation on structural performance predictions of double-bottom tankers during shoal grounding accidents. Marine Structures. 2013;33:188-213.

[9] Manolakos DE, Mamalis AG. Limit analysis for laterally loaded stiffened plates. International Journal of Mechanical Sciences. 1988;30:441-7.
[10] Jiang J, Olson MD. Rigid-plastic analysis of underwater blast loaded stiffened plates. International Journal of Mechanical Sciences. 1995;37:843-59.
[11] Schubak RB, Olson MD, Anderson DL. Nonlinear Rigid-Plastic Analysis of Stiffened Plates under Blast Loads 1991.
[12] Louca LA, Pan YG, Harding JE. Response of stiffened and unstiffened plates subjected to blast loading. Engineering Structures. 1998;20:1079-86.
[13] Schubak RB, Olson MD, Anderson DL. Rigid-plastic modelling of blast-loaded stiffened plates—Part I: One-way stiffened plates. International Journal of Mechanical Sciences. 1993;35:289-306.
[14] Schubak RB, Olson MD, Anderson DL. Rigid-plastic modelling of blast-loaded stiffened plates—Part II: Partial end fixity, rate effects and two-way stiffened plates. International Journal of Mechanical Sciences. 1993;35:307-24.
[15] Yang P, Peng Y. Dynamic Response of Blast-Loaded Stiffened Plates by Rigid-Plastic Analysis. ASME 2010 29th International Conference on Ocean, Offshore and Arctic Engineering: American Society of Mechanical Engineers; 2010. p. 991-9.
[16] Amdahl J. Static resistance of stiffened plates subjected to explosions. FABIG Newsletter Issue 2005;41(R531):4–7. 2005.
[17] Daley CG, Daley KH, Dolny J, Quinton BWT. Overload response of flatbar frames to ice loads. Ships Offshore Struct. 2016:1-14.
[18] Daley C, Hermanski G. Ship frame research program-a experimental study of ship frames and grillages subjected to patch loads. Washington, DC, USA: US Ship Structures Committee, SSC-457. 2009.
[19] Kim H. An experimental study of the design and overload capacity of structural grillages subjected to ice loads [Master thesis]: Master thesis, Memorial University of Newfoundland; 2014.
[20] Jones N. Influence of in-plane displacements at the boundaries of rigid-plastic beams and plates. International Journal of Mechanical Sciences. 1973;15:547-61.
[21] Hodge Jr PG. Post-yield behavior of a beam with partial end fixity. International Journal of Mechanical Sciences. 1974;16:385-8.
[22] De Oliveria J. The behavior of steel offshore structures under accidental collisions. Offshore Technology Conference: Offshore Technology Conference; 1981.
[23] DNV. 'Rules for classification of ships' Ships for navigation in ice. Det NORSKE VERITAS, Norway, Part 5, Chap 1. 2001.
[24] Tørnqvist R. Design of crashworthy ship structures: Technical University of Denmark Kgns Lyngby,, Denmark; 2003.
[25] Pedersen PT, Zhang S. On impact mechanics in ship collisions. Marine Structures. 1998;11:429-49.
[26] Liu Z, Amdahl J. A new formulation of the impact mechanics of ship collisions and its application to a ship–iceberg collision. Marine Structures. 2010;23:360-84.
[27] Biggs JM. Introduction to structural dynamics: McGraw-Hill College; 1964.